Title:

Distinct pathogenic roles for resident and monocyte-derived macrophages in lupus nephritis

Authors:

Nathan Richoz[1,2,3]†, Zewen K. Tuong[1,2,4]†, Kevin W. Loudon[1,2], Eduardo Patiño-Martínez[3], John R. Ferdinand[1,2], Anais Portet[1,2], Kathleen Bashant[3], Emeline Thevenon[5], Francesca Rucci[5], Thomas Hoyler[5], Tobias Junt[5], Mariana J. Kaplan[3], Richard Siegel[3,5]‡, Menna R. Clatworthy[1,2,4]‡

Affiliations:

[1]Molecular Immunity Unit, University of Cambridge Department of Medicine, MRC-Laboratory of Molecular Biology, Cambridge, UK.

[2]Cambridge Institute of Therapeutic Immunology and Infectious Diseases, University of Cambridge, UK.

[3]National Institute of Arthritis and Musculoskeletal and Skin Diseases, National Institutes of Health, Bethesda, Maryland, USA

[4]Cellular Genetics, Wellcome Sanger Institute, Hinxton, UK.

[5]Novartis Institutes for BioMedical Research, Basel, Switzerland.

†equal contribution

‡Corresponding authors

Address for correspondence:
Molecular Immunity Unit, University of Cambridge Department of Medicine
MRC Laboratory of Molecular Biology,
Cambridge Biomedical Campus,
Francis Crick Avenue,
Cambridge. CB2 0QH.
Phone: 44-1223-267279

Email: mrc38@cam.ac.uk

Abstract:

Lupus nephritis is a serious complication of systemic lupus erythematosus (SLE), mediated by IgG immune complex (IC) deposition in kidneys, with limited treatment options. Kidney macrophages are critical tissue sentinels that express IgG-binding Fcγ-receptors (FcγR), with previous studies identifying prenatally-seeded resident macrophages as the major IC responders. Using single cell transcriptomic and spatial analyses in murine and human lupus nephritis, we sought to understand macrophage heterogeneity and subset-specific contributions in disease. In lupus nephritis, the cell fate trajectories of tissue-resident (TrMac) and monocyte-derived (MoMac) kidney macrophages were perturbed, with disease-associated transcriptional states indicating distinct pathogenic roles for TrMac and MoMac subsets. Lupus nephritis-associated MoMac subsets showed marked induction of FcγR-response genes, avidly internalised circulating IC, and presented IC-opsonised antigen. In contrast, lupus-associated TrMac subsets demonstrated limited IC uptake, but expressed monocyte chemoattractants, and their depletion attenuated monocyte recruitment to the kidney. TrMac also produced B cell tissue niche factors, suggesting a role in supporting autoantibody-producing lymphoid aggregates. Extensive similarities were observed with human kidney macrophages, revealing cross-species transcriptional disruption in lupus nephritis. Overall, our study suggests a division of labour in the kidney macrophage response in lupus nephritis, with treatment implications — TrMacs orchestrate leukocyte recruitment while MoMacs uptake and present IC-antigen.

Key words:

Macrophages, kidney, lupus nephritis, IgG, Fcgamma receptor, immune complex, single cell RNA sequencing, BAFF.

Introduction

All tissues contain a network of mononuclear phagocytes (MNP), including macrophages and dendritic cells (DCs) (1), tissue sentinels that express a range of receptors to enable pathogen recognition, including IgG-opsonised microbes. However, this capacity may also promote deleterious inflammation and tissue damage in the context of autoimmunity, for example, by binding autoreactive IgG immune complexes (IC) in patients with systemic lupus erythematosus (SLE). One of the most serious manifestations of SLE is lupus nephritis, a condition characterised by IgG IC deposition in the kidney, activating complement and local immune cells, including macrophages, by engaging Fc-gamma receptors (FcγRs) (2-4). Macrophage IgG IC stimulation results in the generation of proinflammatory cytokines and mediators (5, 6), therefore unsurprisingly, *FCGR* polymorphisms that augment FcγR-mediated macrophage activation are associated with susceptibility to SLE and lupus nephritis (5, 7). In established lupus nephritis, B/plasma cell aggregates capable of local autoantibody production have also been described (8, 9). Current treatments for SLE largely consist of non-specific immunosuppressants, with blockade of the B cell survival cytokine, BAFF (B cell activating factor of the TNF receptor family), the only new therapeutic option (10). A better understanding of cell type-specific responses in lupus nephritis is needed to identify new and more targeted treatments.

Tissue macrophages are seeded into organs prenatally from yolk sac or fetal liver progenitors and are variably replaced postnatally by monocyte precursors (11, 12) (13). Early fate mapping and parabiosis studies suggested that in adult mouse kidney around half of macrophages are prenatally seeded tissue resident cells (TrMac), do not circulate, and express high levels of F4/80, whilst monocyte-derived kidney macrophages (MoMac) have low F4/80 expression and are CD11b high (11). More recent parabiosis experiments confirmed little exchange of F4/80^{hi} cells (14, 15), although kidney injury or pathology may influence the extent to which renal macrophages are replenished from different precursors (16, 17).

Macrophages adopt tissue-specific transcriptional profiles within organs (18). Recent single cell RNA sequencing (scRNAseq) studies showed that MoMac within lung, heart, liver and skin progress along two distinct cell fates, occupying different anatomical niches within the tissues (19); Lyve1^{lo}MHCII^{hi} cells lie adjacent to nerve fibres, and Lyve1^{hi}MHCII^{lo} cells co-localise with vasculature, protecting against the development of fibrosis. The kidney is a highly vascularized organ, necessitated by its homeostatic role of waste and acid removal from blood, but whether MoMac in the kidney differentiate along these two distinct cell fate trajectories, and how this might be perturbed in lupus nephritis is currently unclear.

Previous data suggest that F4/80^{hi} prenatally-seeded TrMac are the cells within the kidney that take up circulating IC, acquiring them from endothelial cells to which they are closely opposed (17, 20). Notably, these studies used model IC, where the antigen-antibody ratio used would generate small IC, whereas medium and large immune complexes are commonly observed in lupus (21, 22). In addition, the IC used in these studies did not contain nucleic acids or DNA (that can activate other innate receptors (23, 24)), and may therefore not truly re-capitulate kidney macrophage responses in lupus nephritis. Here, using a combination of flow cytometric analysis, high dimensional imaging, spatial transcriptomics (ST) and single cell RNAseq, we sought to delineate kidney macrophage heterogeneity, activation, signalling networks, and cell fate trajectories in a murine model of SLE, the MRL/*MpJ-Fas*^{lpr}/J (MRL-*Lpr*) mouse, and to integrate this information with publicly available single cell transcriptional data from human lupus nephritis to identify novel, cell type-specific therapeutic targets.

Results

Expanded kidney macrophage populations in lupus nephritis

We profiled kidney macrophages in MRL-*Mpj* controls and in diseased MRL-*Lpr* mice that harbour a mutation in *Fas* which leads to the survival of autoreactive lymphocytes, the development of anti-nuclear/anti-DNA antibodies and an IC-mediated glomerulonephritis, modelling lupus nephritis (25). Flow cytometric assessment indicated two major kidney MNP populations, an F4/80^{hi} CD11b^{int} population (MNP1) and a F4/80^{lo} CD11b^{hi} population (MNP2), previously reported to be yolk sac- or HCS/monocyte-derived respectively (11), in both MRL and C57BL/6 mice (**Fig. 1A-B**). In all strains examined, the MNP2 subset included an MHCII positive and negative population, referred to hereafter as MNP2+ and MNP2- (**Fig. 1B, C**). In contrast to the previous description that two distinct populations of MoMac in lungs, heart, liver and skin demonstrate binary expression of MHCII, LYVE-1, and CX3CR1 in homeostasis (19), kidney MNP2+ and MNP2- populations expressed similar levels of LYVE1 and CX3CR1 (**Fig. 1C**).

In MRL-*Lpr* mice, a distinct subset of F4/80^{hi} cells was evident, with lower expression of CD11b (designated MNP1^{CD11b-}) (**Fig. 1A, D**). MNP1^{CD11b-} were infrequent in control kidneys, increased with age (**Fig. 1D-E**), and were expanded in other models of antibody-mediated nephritis (NZM2328 and nephrotoxic nephritis) (**Fig 1F**). In addition to this expanded MNP1^{CD11b-} population, MNP2- were also increased in the kidneys of MRL-*Lpr* mice (**Fig. 1D**), suggesting an increase in both MoMac and TrMac populations in lupus nephritis.

Spatially, in control kidneys (both MRL-*Mpj* and C57BL/6), MNP subsets were asymmetrically distributed, with CD11b^{hi} MNPs enriched in the outer medulla, and present in occasional clusters in the cortex and around glomeruli, whilst F4/80^{hi} CD11b$^{int/lo}$ predominated in the

cortex (**Fig. 1G-H, S1A-B**). CD11b^{hi}MHCII+ cells were observed adjacent to interlobular arteries, peritubular capillaries and nerves (**Fig. 1G, S1A**). Thus, MHCII and LYVE1 do not appear to mark macrophages located adjacent to nerves or blood vessels respectively in the kidney. In MRL-*Lpr* kidneys, extensive cortical F4/80- CD11b^{hi} infiltrates were prominent, with some large aggregates that included F4/80^{hi} CD11b- cells (**Fig. 1H**). In addition, F4/80^{hi} CD11b- cells prominently encased every glomerulus (**Fig. 1H, S1B**), altogether consistent with the increase in MNP1^{CD11b-} and MNP2- identified by flow cytometric assessment (**Fig. 1C, D**).

Nephritis-associated macrophage heterogeneity at single cell resolution

To more comprehensively characterise kidney MNP heterogeneity in health and to explore how these populations change in lupus nephritis, we performed droplet encapsulation scRNAseq (*Chromium 10x*), on flow-sorted kidney macrophages isolated from MRL-*MpJ* and MRL-*Lpr* mice (6) (**Fig. 2A**). Sub-clustering of the two major groups we described previously (Group 1 (MNP1) and Group 2 (MNP2)), revealed nine cell clusters (**Fig. 2A**). Notably, MNP1 clusters expressed *Adgre* (F4/80) but little *Itgam* (CD11b), and *vice versa* MNP2 clusters showed minimal expression of *Adgre* (F4/80) but expressed *Itgam* (CD11b) (**Fig. 2B**), analogous to the two major macrophage populations identified by flow cytometry. Group 2 MNPs included a monocyte cluster (2.1), as well as an MHCII-positive (MNP2.2) and -negative (MNP2.3) cluster (**Fig. 2B-C**), mirroring MNP2+ and MNP2- subsets identified by flow cytometry (**Fig. 1**) and the MoMac populations identified in other organs using scRNAseq (19). All MNP1 clusters showed transcriptional similarity with a reference fate-mapped, yolk sac-derived kidney macrophage signature (11) and MNP2 clusters with a fate-mapped kidney monocyte-derived macrophage signature (**Fig. 2D**).

Differentially expressed genes in MNP1.6 included cell cycle genes (**Fig. 2E**), indicating proliferating cells, and other canonical macrophage and monocyte markers (*Itgax* (CD11c), *Cd14*, *Ly6c, Ccr2,* and *Cx3cr1* showed distinct expression patterns with little expression of DC-associated markers (**Fig. 2E**). Each cluster contained cells from both control and diseased kidneys, although MNP1.4 (which did not express *Itgam,* **Fig. 2B**) and MNP2.3 were markedly enriched in diseased samples (**Fig. 2C**), consistent with our flow cytometric and confocal imaging studies which also demonstrated an expansion of subsets of F4/80^{hi} macrophages (MNP1^{CD11b-}), and CD11b^{hi} MHCII- macrophages (MNP2-) in MRL-*Lpr* kidneys (**Fig. 1**).

We next used spatial transcriptomics (ST) to delineate the anatomical localisation of macrophage subsets in homeostasis. Podocyte (*Nphs2*), proximal tubular (*Slc22a13, Slc34a1*), and distal tubule/collecting duct (*Kcnj1, Aqp2*) gene expression delineated the anatomical regions of the kidney (**Fig. 2F, S2A-B**). In control kidneys, group 1 MNP subset

signatures were predominantly enriched in the cortex, except for the proliferating MNP1.6 genes, which enriched in the medulla (**Fig. 2G, S2C**). Group 2 MNP signatures showed distinct localisation patterns, with MNP2.1 (monocytes) signatures enriched in the pelvic region, MNP2.2 in the outer medulla, whilst high MNP 2.3 signatures were scattered around the cortex (**Fig. 2H, S2D**). Using a podocyte signature (Park *et al.*) to specifically select glomerulus-containing voxels (**Fig. 2I)**, we examined the proportion of group 1 and 2 MNPs that localised to glomeruli and found a large increase in glomerular-associated MNP2.3 signatures in the MRL-*Lpr* compared to the MRL-*Mpj* kidney (**Fig. 2J**), consistent with a contribution to glomerulonephritis.

Kidney macrophages show deranged cell state trajectories in lupus nephritis

The developmental trajectories of the F4/80^{hi} Group 1 clusters showed a progression from the proliferating cluster MNP1.6, though to MNP1.5 and then a binary divergence to either MNP1.2 and MNP1.1 or to MNP1.4 and MNP1.3 (**Fig. 3A**), with a marked skewing towards the latter trajectory in MRL-*Lpr* kidneys (**Fig. 3A, S3A**). Transcription factor (TF) regulon activity analysis at the divergence of pseudotime cell fate showed *Maf*, *Runx1, Nfatc2*, *Irf4* and *Irf7* regulated genes were highly expressed by cells transitioning from MNP1.5 to MNP1.2 (**Fig. S3B**), while *Cebpg*, *Junb*, *Irf8* and *Stat1* were expressed in cells transitioning from MNP1.5 to MNP1.4 (**Fig. S3B**). Of note, *Maf* (also known as cMaf), together with MafB, desensitize macrophages to proliferative stimuli, such as M-CSF by inhibiting the expression of genes such as *Myc* (26), promoting a quiescent tissue macrophage phenotype. Furthermore, *Maf* and *Nfact2c* have been shown to be up-regulated in renal macrophages as they differentiate from progenitors following seeding in the embryo, with the latter a kidney-specific TF (18). In contrast, IRF8 and STAT1 mediate inflammatory M1 polarization in macrophages (27), activated by IFNγ stimulation (28).

Chakarov *et al.* used scRNAseq to investigate MoMacs in lungs, skin and heart and showed that MHCII+ and MHCII- cells represented two distinct cell developmental fates rather than cells at opposite ends of a cell differentiation spectrum (19). Similarly, in the kidneys, we found that MNP2.2 and MNP2.3 developed from monocytes (MNP2.1) along two distinct trajectories, with the 2.1->2.3 trajectory favoured in lupus nephritis (**Fig. 3B, S3C**). TF regulon activity showed increased expression of Irf4 and Stat6-controlled genes as cells moved from MNP2.1 (monocytes) to MHCII+ MNP2.2 (**Fig.S3D**), TFs known to polarize toward an anti-inflammatory M2 macrophage phenotype (27). In contrast, Stat3-regulated genes increased in cells progressing towards MNP2.3 (MHCII-) cluster (**Fig.S3D**), with STAT3 activated by a number of cytokines, including IL6 (29).

Monocyte-derived macrophages are IC responders in lupus nephritis

Interestingly, NFkB1-regulated genes were also increased in MoMacs as they differentiated from monocytes, a TF activated by FcγR crosslinking in phagocytes (30). (**Fig.S3D**). Indeed, *Fcgr4* (an activating FcγR) expression was substantially higher in MNP2.3 in MRL-*Lpr* compared with MRL-*Mpj* kidneys **(Fig. 3C**), with a marked reduction in the inhibitory *Fcgr2b* in all TrMac and MoMa subsets (particularly MNP2.2) in MRL-*Lpr* kidneys, with the overall effect of increasing macrophage activation upon IgG IC encounter. Consistent with this, we observed a significant enrichment of a macrophage IgG IC-stimulation gene signature across all group 1 and group 2 MNP clusters in MRL-*Lpr* mice compared with MRL-*MpJ* mice, particular in MNP1.5 (**Fig. 3D**). Furthermore, gene ontology (GO)- and Kyoto Encyclopedia of Genes and Genomes (KEGG)- curated genesets for FcγR signalling and FcγR-mediated phagocytosis were strongly enriched in MNP2.3 in MRL-*Lpr* kidneys (**Fig. 3D**). ST analysis confirmed a significant increase in IC-induced gene signatures in MRL-*Lpr* kidneys that co-localised with the MNP1.5 gene signature (**Fig. 3E**), as well as an increase in expression of the FcγR-mediated phagocytosis geneset in the cortex, that co-localised MNP2.3 gene signature (**Fig. 3F**). Together these data support the conclusion that disease-associated subsets of both TrMac and MoMac are responding to IgG IC stimulation via FcγR cross-linking in lupus nephritis.

Given that our single cell RNAseq and ST analysis showing MoMac as IC responders was in contrast to previous reports implicating prenatally seeded TrMac as the principal cell type capable of internalising IC (17, 20), we sought to directly assess the capacity of kidney macrophages to internalise circulating ovalbumin (OVA) immune complexes, generated using varying ratios of rabbit anti-OVA IgG. Following in vivo challenge by intravenous administration of IC, F4/80^{hi} TrMac internalised free OVA and small IC (IgG: OVA ratio of 1:1 and 1:10), but demonstrated little uptake of larger IC (IgG: OVA ratio of 5:1) (**Fig. 4A**). In contrast, MoMac subsets readily internalised large IgG IC from the circulation (**Fig. 4A**). To further confirm that this observation was not limited to rabbit IgG IC, we generated larger IC using mouse anti-OVA IgG and similarly showed that MoMac subsets readily internalised circulating IC with no significant uptake by F4/80^{hi} TrMac in vivo (**Fig. S3E**). In vitro, FcγR-crosslinking by OVA IC and (to an even greater extent) anti-dsDNA-DNA IC induced the production of TNFα, and IL-1β, by both TrMac and MoMac (**Fig. 4B**). In the scRNAseq data, group 1 and group 2 MNPs expressed AIM2, which may contribute to the augmented responses to anti-dsDNA IC (**Fig. S3F**). Both TrMac and MoMac were able to present immune complexed Y-Ae (31) in vitro, but in vivo TrMac did not present IV immune complexed antigen, instead, MoMac were the

major antigen presenters (**Fig. 4C**). Together, these data implicate MoMac as IC-phagocytosing and responding populations in the kidney in vivo.

Tissue-resident macrophages orchestrate monocyte-recruitment in lupus nephritis

We next considered the role of TrMac in lupus pathogenesis. Analysis of cell-cell interactions between mouse TrMac and MoMac subsets based on receptor-ligand expression (32) revealed the potential for MNP1.5 to recruit MNP2.1 via the expression of *Ccl4* and *Ccl8* in MRL-*Lpr* but not MRL-*MpJ* kidneys (**Fig. 5A**). ST analysis confirmed the significance of such interactions in vivo as *Ccl8* and *Ccr5* were shown to be co-expressed in inflamed regions of MRL-*Lpr* kidneys, with *Ccl8* expression colocalising with MNP1.5 gene signatures in these regions (**Fig. 5B**). Similarly, *Ccl8* and *Ccr2* or *Ccl4* and *Ccr5* were also co-expressed in MRL-*Lpr* kidneys, with co-localised expression undetectable in MRL-*MpJ* kidneys (**Fig. 5C**).

In MRL-*Lpr* kidneys, MNP1.4 also expressed *Hebp1* (**Fig. 5A**), a molecule with chemoattractant activity via *Fpr3* (33). *Cd72-Sema4d* mediated interactions were also predicted to re-enforce physical associations between lupus-associated TrMac subsets (MNP1.4 and MNP1.5) and MoMac subsets in the context of nephritis (**Fig. 5A**), which was further supported by the expression of *Sema4d* in large CD11b^{hi} MNP2 infiltrates (**Fig. 5D**) as well as the co-expression of these molecules in MRL-*Lpr* kidneys (**Fig. 5C**). Notably, *Sema4d* (CD100) has previously been shown to promote macrophage accumulation in glomeruli in nephrotoxic nephritis (34), and CD72 ligation by CD100 can directly activate MNPs (35).

To validate the importance of MNP1-MNP2 interactions in vivo following challenge with ICs, we treated mice with liposomal clodronate, which specifically depleted kidney TrMac but had no significant effect on kidney or blood MNP2 numbers (**Fig. 6A-D**). Challenging mice with large ICs intravenously resulted in a significant increase in kidney MoMac, which was substantially abrogated by prior depletion of TrMac with liposomal clodronate (**Fig. 6D**), demonstrating the functional importance of TrMac chemokine production in orchestrating monocyte recruitment in the context of IC stimulation.

Tissue-resident macrophages produce B cell cytokines

In addition to inflammatory cell infiltrates, tertiary lymphoid follicles with B/plasma cell aggregates capable of local autoantibody production have been described in murine models of lupus nephritis (8, 9). We therefore asked whether kidney MNPs expressed B/plasma cell survival factors that might support such activity. We found increased expression of *Tnfsf13b*, (encoding the B/plasma cell survival factor BAFF), in lupus-enriched TrMac subsets (MNP1.3, 1.4 and 1.5) in MRL-*Lpr* kidneys compared with MRL-*MpJ,* with little *Tnfsf13b* expression in

MoMac subsets (**Fig. 7A, S4A).** In the ST data, B cell clusters (evidenced through expression of *Cd79a*), were found in areas with high *Tnfsf13b* expression, and specifically co-localised with MNP1.5 gene signatures (**Fig. 7B**). BAFF expression was also detected at the protein level in F4/80^{hi} MNPs only in kidneys from MRL-*Lpr* mice (**Fig. 7C**), with tertiary lymphoid-like structures formed of B cells, T cells and MNPs evident in inflamed kidneys (**Fig. 7D**).

Human kidney MNP show perturbations in FcyR expression, activation and interactions in lupus nephritis

To validate these findings in human kidney macrophage in SLE, we integrated our dataset of single cell transcriptomes from healthy human kidney macrophages (36) with those isolated from human kidneys with lupus nephritis (37). Macrophages formed three major clusters with expression profiles consistent with their identity as classical monocyte-derived macrophages, non-classical monocyte-derived macrophages, and tissue-resident macrophages, each of which contained cells from both healthy and lupus nephritis kidneys (**Fig. 8A**). The tissue-resident cluster enriched for YS-derived mouse kidney macrophage gene signature, and the monocyte-derived clusters for HSC/monocyte derived mouse kidney macrophage gene signature (**Fig. S4B).** Comparing mouse kidney macrophage transcriptomes to human macrophages, group 1 MNP signatures were enriched in the tissue-resident human macrophage cluster and group 2 MNP signatures were enriched in the human MoMac clusters (**Fig. 8B**). Macrophage IC-stimulation signature genes were increased in all three human macrophage subsets in lupus nephritis compared with healthy kidneys, particularly in classical MoMac (**Fig. 8C**). Furthermore, the MRL-*Lpr*-enriched murine MNP2.3 signature was increased in human MoMac in lupus nephritis, whilst the MRL-*MpJ*-enriched MNP2.2 signature was decreased (**Fig. S4C**).

Interestingly, as observed in murine MRL-*Lpr* MNP1 clusters, *TNFSF13B* (encoding BAFF) expression was increased in tissue-resident macrophages in human lupus nephritis compared with control kidneys (**Fig. 8D**), and macrophage BAFF expression was validated in biopsies obtained from patients with lupus nephritis (**Fig. 8E**). Receptor-ligand expression analysis integrating kidney B cell and macrophage single cell data confirmed BAFF as a major mediator of macrophage-B cell interactions, but revealed differing BAFF receptor expression in lupus nephritis, with *TNFSR13B* (encoding TACI (transmembrane activator and cyclophilin ligand interactor)) prominent in mediating interactions in lupus nephritis but *TNFSR13C* (encoding BAFF-R) dominant in control kidneys (**Fig. 8F-G**).

Monocyte-derived macrophages in lupus nephritis biopsies showed increased expression of *CCR5* and *FRP3* in lupus nephritis (**Fig. S4D**), mirroring our findings in MRL-*Lpr* kidneys, and there was also increased expression of *SEMA4D* in both MoMac and TrMac subsets (**Fig. S4D).** All of the top ten MNP1.4 TF regulons were increased in human tissue-resident

macrophages in lupus nephritis, including *STAT1* (**Fig. S5A**), and many of the top ten MNP2.3 TF regulons were increased in monocyte-derived macrophages (**Fig. S5B**). This included *IKZF1* (encoding IKAROS), a genetic susceptibility locus for human SLE and lupus nephritis (38, 39).

Overall, these data indicate distinct roles for TrMac and MoMac in lupus nephritis, and show similar disruption of kidney macrophage signalling networks in mouse and human, with TrMac promoting monocyte recruitment and providing a tissue niche for B cells (**Fig. S5C**).

Discussion

Our work has several surprising findings; a previous study applying scRNAseq to tissue macrophages found two distinct populations of MoMac in lungs, heart, liver and skin that were MHCII^{hi}/LYVE-1^{lo}, or *vice versa*, that developed along two distinct trajectories and occupied distinct anatomical niches adjacent to nerves and blood vessels respectively (19). The authors suggested this was a universal phenomenon across organs, but although we similarly saw binary fate trajectories in the kidney, these two populations expressed similar levels of LYVE1 and CX3CR1 and did not differentially co-localise with vasculature or nerves. In lupus nephritis, macrophage fate in these MoMac was skewed towards the development of the MHCII-negative subset, that showed increased *Fcgr4* expression, and transcriptional evidence of high NFkB activity and FcγR-mediated activation. This was unexpected, given previous reports suggesting that F4/80^{hi}, prenatally seeded TrMac represent the major population capable of phagocytosing circulating IgG IC (17, 20), but when we directly challenged mice with large IC intravenously, we confirmed that CD11b^{hi} MoMac subsets had substantial capacity to internalise IC in vivo. The likely explanation for these differing observations relates to the size of IgG IC, with previous studies utilising small or monomeric IgG opsonised antigens, whilst we profiled uptake of a range of sizes of IC, includer larger IC that more closely resemble those found in human lupus (21, 22).

While F4/80^{hi} TrMac subsets showed minimal IC uptake, our data indicates an important role in orchestrating tissue inflammation in lupus nephritis. Disease-enriched TrMac subsets expressed chemokines capable of orchestrating the recruitment of monocytes, validated using ST datasets, and shown to be functionally important by the demonstration that TrMac attenuated monocyte recruitment to the kidneys post-intravenous IgG IC challenge. TrMac in mouse and human lupus nephritis also showed increased expression of *TNFSF13B,* encoding BAFF, a cytokine that enhances B cell survival and proliferation (40) and contributes to the plasma cell niche (41). BAFF mediates its effects via three receptors, TNFSFR13C (BAFF-R), TNFSFR17 (BCMA), and TNFSFR13B (TACI). Selective BAFF blockade prevents the development of LN in mice (42) and the humanised anti-BAFF IgG1 antibody belimumab is

licenced for use in patients with SLE (43), with potential efficacy in lupus nephritis (44). Our analysis specifically identified TrMac as a source of kidney BAFF in mice and humans, and implicated TACI in intra-renal B cell responses to BAFF in lupus nephritis but not in homeostasis, highlighting a disease-specific therapeutic target. Both TrMac and MoMac showed increased expression of *SEMA4D* (CD100) in lupus nephritis. Its ligand CD72 is highly expressed by B cells (45), identifying an additional axis of macrophage-B cell cross-talk that may also represent a novel therapeutic target.

In summary, our study presents a detailed analysis of the single cell transcriptional profiles of kidney macrophages in lupus nephritis, integrating murine and human data, and providing spatial validation using ST. We define how cell fate trajectories of both TrMac and MoMac macrophages become deranged in disease, and identify key transcription factors that may control cell progression towards a more pro-inflammatory transcriptional programme. We find distinct roles for TrMac and MoMac, with the former showing limited IC uptake but playing a major role in orchestrating the recruitment and maintenance of inflammation-associated cells, and the latter able to internalise and present IC-associated antigen. Overall, this work provides a single cell and spatial transcriptional atlas for macrophages in lupus nephritis and identifies novel cell-subset specific therapeutic targets.

Methods

Mice

Wild-type C57BL/6 mice were obtained from the Jackson Laboratories. Transgenic mice expressing Venus EYFP under the control of the CD11c promoter were a gift from M. Nussenzweig (Rockefeller University, New York, USA). NZM2328 mice were a gift from M.J. Kaplan (National Institute of Arthritis and Musculoskeletal and Skin Diseases, National Institutes of Health, Bethesda, USA). MRL-MpJ (no. 00486) and MRL-Lpr (no. 00485) mice were obtained from the Jackson Laboratories. In all experiments, both male and female mice were used. For all in vivo experiments, 8- to 16-wk-old mice were used. In the United Kingdom, mice were maintained in specific pathogen-free conditions at a Home Office-approved facility.

Murine kidney processing

Following terminal procedure, mouse kidneys were minced finely and digested in RPMI containing 0,1mg/mL DNAse I, 0,0325mg/mL Liberase TM and 10mM HEPES for 25 minutes at room temperature. Organs were then mechanically dissociated through a 70 µm cell strainer, washed in PBS and red blood cell lysis was performed. Single cell suspension was enriched in hematopoietic cells by Percoll gradient centrifugation (2000rpm in 44% Percoll in RPMI 10% FBS (centrifuge break on 0) for 20 minutes), pellet was washed with cold PBS 2% FBS and cells were then used for further analysis.

Flow cytometry

Single cell suspensions were blocked for 30 minutes with 50µL normal mouse serum in PBS 2% FBS on ice then stained with the appropriate fluorescently labelled antibodies (see antibody table) and live/dead staining for 30 minutes on ice. When using biotinylated antibodies, cells were then washed and stained with fluorescently labelled streptavidin for 20 minutes on ice. After washing, cells were analysed on a LSRFortessa (BD Biosciences). FCS files were analysed using FlowJo v9.9.6. Antibodies used in this study in table S1.

Cell sorting

Stained samples were sorted on a FACSAria III (BD Biosciences) following the appropriate gating strategy. Cells were sorted under the 4-way purity setting into chilled FBS and kept on ice until ready to use.

Generation of OVA immune complexes (ICs)

ICs were prepared in vitro by incubating AlexaFluor647-OVA (1mg/mL in PBS) or DQ-OVA (1mg/mL in PBS) with rabbit polyclonal anti-OVA antiserum (3,7mg/mL) at a 1:10, 1:5, 1:1, 5:1

or 10:1 molar ratio for 60 minutes in a 37°C water bath. Large ICs (1:5 and 1:10 molar ratios) were washed twice (10000rpm for 2 minutes and discard the supernatant) prior to be injected to remove excess OVA or excess IgG.

Generation of DNA ICs

ICs were prepared in vitro by incubation Ultrapure salmon sperm DNA (Thermofisher) sonicated into fragments ranging from 150 to 300bp with anti-dsDNA antibodies engineered to have a human IgG1 backbone for 60 minutes in a 37°C water bath. The anti-dsDNA antibodies were provided Drs. Thomas Hoyler and Tobias Junt from the autoimmunity, transplantation and inflammation branch at Novartis, Switzerland.

In vitro uptake by kidney MNPs

Single cell suspension was prepared as described. Cells were then resuspended in pre-warmed RPMI 10% FBS and plated in a 24-well plate, 3x106 cells per well in 300µL medium. Cells were given opsonized/free ovalbumin in 10µL PBS and incubated in the dark at 37°C for the appropriate time. After incubation, cells were washed with cold PBS 2% FBS and stained for flow cytometry analysis.

In vivo uptake by kidney MNPs

All compounds were administered i.v. via tail vein injection in a final volume of 100 µL. ICs of different sizes were prepared as described so that each mouse receives 8µg worth of AF647-OVA. The amount of anti-OVA serum used to form immune complexes was calculated to fit the desired molar ratios. Two hours after injection, mice were culled via cervical dislocation. Both kidneys and blood from the renal vein were harvested for further processing.

Antigen presentation

Eα peptide (sequence CGGGASFEAQGALANIAVDKA) was conjugated to AF647-OVA (termed Eα-OVA) on custom order (ALMAC, UK). Eα-OVA was mixed at a 1:1 ratio with AF647-OVA for all antigen presentation experiments. Presentation was assessed using the Yae antibody clone for flow cytometry.

Confocal microscopy of human samples

Biopsies were processed and embedded in paraffin. Before staining, 10µm sections were heated 30 min at 65 °C and then rehydrated as follow: Xylene - 10 min, two changes; 100 % ethanol - 10 min, two changes; 95 % ethanol - 5 min, 70 % ethanol - 5 min, 50 % ethanol - 5 min, washed with deionized water and rehydrated with PBS 1X - 10 min. Antigen retrieval was perform using Citrate buffer 100X pH 6.0 (ab93678) 99 °C – 40 min. Sections were incubated

with primary for 2h at RT and washed 3 times in PBS. Finally, sections were incubated with the appropriate fluorochrome-labeled secondary antibodies for 1h at RT, washed in PBS and mounted in Fluoromount-G with DAPI (Invitrogen). Images were acquired using a TCS SP8 (Leica microsystems) confocal microscope. Raw imaging data were processed using Imaris (Bitplane). Antibodies used in this study in table S1.

Confocal microscopy of murine samples

Samples were fixed in 1% paraformaldehyde (Electron Microscopy Services) / L-lysine/ sodium periodate (both Sigma-Aldrich) buffer for 24 hr or in AntigenFix for 1h at 4°C followed by 8 hr in 30% sucrose in PBS. 30µm sections were permeabilized and blocked in 0.1M TRIS, containing 0.1% Triton (Sigma), 1% normal mouse serum, 1% normal rat serum and 1% BSA (R&D systems). Samples were stained for 2h at RT in a wet chamber with the appropriate antibodies, washed 3 times in PBS and mounted in Fluoromount-G® (Southern Biotech). Images were acquired using a TCS SP8 (Leica microsystems, Milton Keynes, UK) inverted confocal microscope, on a 40x 1.3N/A oil or 40x 1.1N/A water objective. Raw imaging data were processed using Imaris (Bitplane). Antibodies used in this study in table S1.

Iterative staining

Iterative staining of sections was performed as previously described (46, 47). Samples were prepared and stained as described above. Following acquisition, the coverslip was removed and slides were washed 3 times in PBS to remove any mounting medium. Bleaching of the fluorochromes was achieved using a 1mg/mL solution of lithium borohydride in water (Acros Organics) for 15 minutes at RT. The slides were then washed 3 times in PBS prior to staining with a different set of antibodies as described above. The process was repeated up to 5 times. Raw imaging data were processed using Imaris (Bitplane) using Hoechst or CD31 as fiducial for the alignment of subsequent images.

Production of anti-OVA antibodies in mouse

Mice were immunized subcutaneously with 100µL of OVA in Incomplete Freund's Adjuvant (IFA) (50µg of OVA per immunization) on day 0 and day 14. On day 28, mice were culled via CO2 and blood was collected into serum separation tubes (Sarstedt) via cardiac puncture. After 30 minutes at room temperature, the tubes were centrifuged at 10rpm for 5 minutes and serum was collected for later IgG purification.

IgG purification from serum

Serum from OVA-immunized mice was collected as previously described. IgG were purified using the Pierce Protein A IgG purification kit following the manufacturer's protocol, using

sterile PBS as binding/washing buffer, 0.1M glycine with 150mM NaCl, pH 2.5 as elution buffer and 1M Tris, pH 7 as neutralization buffer. IgG content was measured on a Nanodrop 2000 (Thermo Scientific). Amicon Ultra 15mL centrifugal filters (Merck) were used to exchange buffer for sterile PBS and the purified IgG solution was kept at -20°C until required.

Nephrotoxic nephritis

Mice were given a single intravenous injection of 50µL sheep anti-rat isolated glomerular basement membrane serum (ProbeTex, USA) on day 0. Proteinuria was monitored daily using Uristix 11 from day 1 and the mice were euthanized for analysis on day 4.

Cell collection and library preparation for single-cell sequencing

Cells were flow sorted as previously described and centrifuged at 1300rpm for 5 minutes. Supernatant was discarded and the pellet resuspended in PBS 0.05% BSA. Cells were loaded at an appropriate concentration to enable recovery of 10 000 cells. 10x single cell 3' v2 kit as per the manufacturer's protocol. Libraries were produced using the manufactures protocol and sequenced on a HiSeq 4000 (Illumina).

Single-cell data analysis and preprocessing - mouse

Single-cell gene expression data from cellranger output was analysed using standard Seurat-inspired scanpy (v.1.4.5.post2) workflow (48, 49). Doublet detection was performed using scrublet (v0.2.1) (50) with adaptations outlined in (51) – Briefly, after scrublet was performed, the data was iteratively sub-clustered using standard Seurat-inspired scanpy (v.1.4.5.post2) workflow (48, 49) and a median scrublet score for each sub-cluster was computed. Median absolute deviation (MAD) scores were computed from the cluster scrublet scores and a one tailed t-test was performed with Benjamini-Hochberg (BH) correction (52) applied and cells with significantly outlying cluster scrublet scores (BH pval < 0.1) were flagged as potential doublets. The data was then processed using scanpy with standard quality control steps; cells were filtered if number of genes > 2500 or < 200. Percentage mitochondrial content cut-off was set at <5%. Genes were retained if they are expressed by at least 3 cells. Genes counts for each cell were normalized to contain a total count equal to the median of total counts in cells before normalization. This led to a working dataset of 3,654 cells. Highly variable genes were selected based on the following parameters: minimum and maximum mean expression are >=0.0125 and <=3 respectively; minimum dispersion of genes = 0.5. The number of principal components used for neighbourhood graph construction and dimensional reduction was set at 50. Batch correction was performed using bbknn with strains as the batch term with all other parameters as per default settings (53). Clustering was performed using Leiden algorithm (54) with resolution set at 1.0. Uniform Manifold Approximation and Projection

(UMAP; v3.10.0) (55) was used for dimensional reduction and visualization, the minimum distance was set at 0.3 and all other parameters as per default settings in scanpy.

Single-cell data analysis - human

Normalized single-cell data from normal and lupus nephritis human kidneys were downloaded from (36) and (37). The two datasets were integrated with ingest protocol in scanpy.

Differential gene testing

Differential gene testing was performed using the Wilcoxon test rank sum test implemented in scanpy's rank_genes_groups module.

Gene set testing

Gene set testing was performed using AUCell analysis tool (56). Genes sets from the respective studies were downloaded from: ArrayExpress (YS vs HSC signature, E-MEXP-3510; MSigDB (57, 58) (GO_FC_GAMMA_RECEPTOR_SIGNALING_PATHWAY, KEGG_FC_GAMMA_R_MEDIATED_PHAGOCYTOSIS, GSE7509_FCGRIIB_STIM_MONOCYTE_ DOWN and GSE7509_FCGRIIB_STIM_DC_ DOWN (59)); interferon signatures (60); macrophage stimulation signatures (61); opsonized immune complex signatures (62). Heatmaps were generated using the pheatmap R package.

Cell type similarity assessment

We used a logistic regression approach to test for cell type similarity with Lyve1+/Lyve1- macrophages from (19). This is done with L2-regularized logistic regression (ridge regression) binomial model with the glmnet R package (63) (i.e. alpha parameter = 0). Models were trained on normalized gene expression data with 10-fold cross-validation to obtain the appropriate lamda coefficient (lambda.1se; within 1 standard error from best model) for prediction. Genes were filtered for tissue specific genes as per (19) prior to model training. Gene expression values were standardized in both the training and test sets. The average of 50 iterations was used for the final score.

Trajectory analyses

Cell trajectory analyses were performed using slingshot (64) and tradeSeq (65). The cells were ordered based on the root node closest to clusters dimed to be comprised of proliferating/dividing cells (Group1.6) or monocytes (Group2.1). PCA was used for learning the trajectory.

Transcription factor enrichment analysis

Transcription factor and regulon enrichment was performed using pyscenic (66). The top 10 cluster specific regulons were determined by calculating regulon specificity scores and significantly different enriched regulons based on wilcoxon rank sum tests between clusters of interest (Group1.4 vs Group1.2 and Group2.3 vs Group2.2).

CellPhoneDB analysis

Normalised expression values from macrophage cell types found in this dataset, as well as ine were subjected to CellPhoneDB analysis (v2.0.0) (67). The minimum threshold was set at 30% and results were considered statistically significant if $p < 0.05$.

Spatial transcriptomic analysis

Analysis of Visium Spatial Gene Expression data was performed using Seurat v3.2.3 as per default methods. Prediction/label transfer was performed using the default SCTransform protocol. Correlation of molecules on the Visium data was performed by computing the correlation score across overlapping k-nearest neighborhoods of a spot based on spatial coordinates, followed by averaging across the neighborhoods. If any neighborhoods return with NA values, due to uniform expression values across the entire neighboorhood, the correlation value will not be returned and visualized as a grey spot. Only positive correlation values are retained for the the analysis.

Transcriptomic data visualization

Mean expression dot plot: size of circle indicates the percentage of cells expressing the genes and increasing expression (scaled from 0 to 1) corresponds to increasing colour gradient from white to blue (**Fig. 2B, S3F**) or from purple, blue, green to yellow (**Fig. 2E, 3C**).

Heatmap: Row/column enrichment value is scaled from 0 to 1 and presented as an increasing gradient from white to blue (**Fig. 2D**) or from purple, blue, green to yellow (**Fig. 3D, 8B-C**) which corresponds to increasing enrichment score.

CellPhoneDB: The order of the receptor-ligand interactions corresponds to the order of the cell-types i.e. celltype A expressing molecule A interacts with celltype B expressing molecule B. Size of circles and color gradient corresponds to the receptor-ligand interaction score, which purple, blue, green to yellow for increasing values (**Fig. 5A, 8F**).

Spatial transcriptomics: Expression of molecules/genes per spot are colored from increasing gradient from purple to green to yellow to red (**Fig. 2F, 7B**) or from white to red (**Fig. 3E-F, 5B)** and corresponds to increasing expression value.

Statistical analyses

Statistical analyses were performed in R, python or Prism where appropriate. For the single-cell data analyses, in general, non-parametric tests were used and stated in the corresponding figure legends. BH or Bonferroni post-hoc correction procedure is applied for multiple testing correction and adjusted p-value < 0.05 were considered statistically significant. Dot plots represent mean ± SD.

Study approval

All animal procedures were conducted in accordance with the United Kingdom Animals (Scientific Procedures) Act of 1986. In the United States, all animal study protocols were approved by the animal care and use committee (ACUC) of the National Institute of Arthritis and Musculoskeletal and Skin Diseases, listed on animal study protocol AO14-01–01, and in agreement with ARAC guidelines (3.18.1).

Kidney biopsies from 3 patients with a diagnosis of Lupus Nephritis (LN III/IV/V each) and 3 healthy portions of kidneys obtained during nephrectomy of subjects with a diagnosis of renal cell carcinoma were obtained through NIH protocol 94-AR-0066. All tissue samples were obtained in accordance with the Ethics Committee procedures, and all patients provided written informed consent.

Author contribution:

Research study design was contributed by NR, MJK, RS and MRC. Conducting experiment was contributed by NR, KWL, EPM, JRF and AP. Data analysis was contrtibuted by NR and ZKT. KB, ET, FR, TH and TJ provided reagents. NR (first) and ZKT (second) are co-first authors based on their degrees of contribution.

Acknowledgements:

We thank Elisabetta Traggiai for useful discussions about the use of anti-DNA antibodies. NR is funded by a Wellcome NIH PhD Fellowship (106809/Z/15/Z). ZKT and MRC are supported by a Medical Research Council Research Project Grant (MR/S035842/1). JRF and MRC are supported by the National Institute of Health Research (NIHR) Cambridge Biomedical Research Centre and the NIHR Blood and Transplant Research Unit and MRC by a Medical Research Council New Investigator Research Grant (MR/N024907/1), a Versus Arthritis Cure Challenge Research Grant (21777), and a Wellcome Investigator Award (220268/Z/20/Z). KB and MJK are supported by the intramural research program at NIAMS/NIH (ZIA AR041199), and RS was supported by NIAMS (ZIA AR041133).

Conflicts of interest:

TJ, ET, and RS are employees of Novartis and own Novartis stock.

References:

1. Guilliams M, Ginhoux F, Jakubzick C, Naik SH, Onai N, Schraml BU, et al. Dendritic cells, monocytes and macrophages: a unified nomenclature based on ontogeny. *Nat Rev Immunol.* 2014;14(8):571-8.
2. Rahman A, and Isenberg DA. Systemic lupus erythematosus. *N Engl J Med.* 2008;358(9):929-39.
3. Clatworthy MR, and Smith KG. B cells in glomerulonephritis: focus on lupus nephritis. *Semin Immunopathol.* 2007;29(4):337-53.
4. Smith KGC, and Clatworthy MR. FcgammaRIIB in autoimmunity and infection: evolutionary and therapeutic implications. *Nat Rev Immunol.* 2010;10(5):328-43.
5. Floto RA, Clatworthy MR, Heilbronn KR, Rosner DR, MacAry PA, Rankin A, et al. Loss of function of a lupus-associated FcgammaRIIb polymorphism through exclusion from lipid rafts. *Nat Med.* 2005;11(10):1056-8.
6. Jing C, Castro-Dopico T, Richoz N, Tuong ZK, Ferdinand JR, Lok LSC, et al. Macrophage metabolic reprogramming presents a therapeutic target in lupus nephritis. *Proc Natl Acad Sci U S A.* 2020;117(26):15160-71.
7. Willcocks LC, Smith KG, and Clatworthy MR. Low-affinity Fcgamma receptors, autoimmunity and infection. *Expert Rev Mol Med.* 2009;11:e24.
8. Cassese G, Lindenau S, de Boer B, Arce S, Hauser A, Riemekasten G, et al. Inflamed kidneys of NZB / W mice are a major site for the homeostasis of plasma cells. *Eur J Immunol.* 2001;31(9):2726-32.
9. Espeli M, Bokers S, Giannico G, Dickinson HA, Bardsley V, Fogo AB, et al. Local Renal Autoantibody Production in Lupus Nephritis. *J Am Soc Nephrol.* 2010.
10. Smith RM, Clatworthy MR, and Jayne DR. Biological therapy for lupus nephritis-tribulations and trials. *Nat Rev Rheumatol.* 2010;6(9):547-52.
11. Schulz C, Gomez Perdiguero E, Chorro L, Szabo-Rogers H, Cagnard N, Kierdorf K, et al. A lineage of myeloid cells independent of Myb and hematopoietic stem cells. *Science.* 2012;336(6077):86-90.
12. Ginhoux F, and Guilliams M. Tissue-Resident Macrophage Ontogeny and Homeostasis. *Immunity.* 2016;44(3):439-49.
13. Liu Z, Gu Y, Chakarov S, Bleriot C, Kwok I, Chen X, et al. Fate Mapping via Ms4a3-Expression History Traces Monocyte-Derived Cells. *Cell.* 2019;178(6):1509-25 e19.
14. Sheng J, Ruedl C, and Karjalainen K. Most Tissue-Resident Macrophages Except Microglia Are Derived from Fetal Hematopoietic Stem Cells. *Immunity.* 2015;43(2):382-93.
15. Lever JM, Yang Z, Boddu R, Adedoyin OO, Guo L, Joseph R, et al. Parabiosis reveals leukocyte dynamics in the kidney. *Lab Invest.* 2018;98(3):391-402.
16. Salei N, Rambichler S, Salvermoser J, Papaioannou NE, Schuchert R, Pakalniskyte D, et al. The Kidney Contains Ontogenetically Distinct Dendritic Cell and Macrophage Subtypes throughout Development That Differ in Their Inflammatory Properties. *J Am Soc Nephrol.* 2020;31(2):257-78.
17. Liu F, Dai S, Feng D, Qin Z, Peng X, Sakamuri S, et al. Distinct fate, dynamics and niches of renal macrophages of bone marrow or embryonic origins. *Nat Commun.* 2020;11(1):2280.
18. Mass E, Ballesteros I, Farlik M, Halbritter F, Gunther P, Crozet L, et al. Specification of tissue-resident macrophages during organogenesis. *Science.* 2016;353(6304).

19. Chakarov S, Lim HY, Tan L, Lim SY, See P, Lum J, et al. Two distinct interstitial macrophage populations coexist across tissues in specific subtissular niches. *Science.* 2019;363(6432).
20. Stamatiades EG, Tremblay ME, Bohm M, Crozet L, Bisht K, Kao D, et al. Immune Monitoring of Trans-endothelial Transport by Kidney-Resident Macrophages. *Cell.* 2016;166(4):991-1003.
21. Cairns SA, London A, and Mallick NP. The value of three immune complex assays in the management of systemic lupus erythematosus: an assessment of immune complex levels, size and immunochemical properties in relation to disease activity and manifestations. *Clin Exp Immunol.* 1980;40(2):273-82.
22. Tung KS, DeHoratius RJ, and Williams RC. Study of circulating immune complex size in systemic lupus erythematosus. *Clin Exp Immunol.* 1981;43(3):615-25.
23. Paludan SR, and Bowie AG. Immune sensing of DNA. *Immunity.* 2013;38(5):870-80.
24. Ablasser A, and Hur S. Regulation of cGAS- and RLR-mediated immunity to nucleic acids. *Nat Immunol.* 2020;21(1):17-29.
25. Adachi M, Watanabe-Fukunaga R, and Nagata S. Aberrant transcription caused by the insertion of an early transposable element in an intron of the Fas antigen gene of lpr mice. *Proc Natl Acad Sci U S A.* 1993;90(5):1756-60.
26. Soucie EL, Weng Z, Geirsdottir L, Molawi K, Maurizio J, Fenouil R, et al. Lineage-specific enhancers activate self-renewal genes in macrophages and embryonic stem cells. *Science.* 2016;351(6274):aad5510.
27. Lawrence T, and Natoli G. Transcriptional regulation of macrophage polarization: enabling diversity with identity. *Nat Rev Immunol.* 2011;11(11):750-61.
28. Hu X, and Ivashkiv LB. Cross-regulation of signaling pathways by interferon-gamma: implications for immune responses and autoimmune diseases. *Immunity.* 2009;31(4):539-50.
29. Niemand C, Nimmesgern A, Haan S, Fischer P, Schaper F, Rossaint R, et al. Activation of STAT3 by IL-6 and IL-10 in primary human macrophages is differentially modulated by suppressor of cytokine signaling 3. *J Immunol.* 2003;170(6):3263-72.
30. Tridandapani S, Wang Y, Marsh CB, and Anderson CL. Src homology 2 domain-containing inositol polyphosphate phosphatase regulates NF-kappa B-mediated gene transcription by phagocytic Fc gamma Rs in human myeloid cells. *J Immunol.* 2002;169(8):4370-8.
31. Murphy DB, Rath S, Pizzo E, Rudensky AY, George A, Larson JK, et al. Monoclonal antibody detection of a major self peptide. MHC class II complex. *J Immunol.* 1992;148(11):3483-91.
32. Vento-Tormo R, Efremova M, Botting RA, Turco MY, Vento-Tormo M, Meyer KB, et al. Single-cell reconstruction of the early maternal-fetal interface in humans. *Nature.* 2018;563(7731):347-53.
33. Migeotte I, Riboldi E, Franssen JD, Gregoire F, Loison C, Wittamer V, et al. Identification and characterization of an endogenous chemotactic ligand specific for FPRL2. *J Exp Med.* 2005;201(1):83-93.
34. Li M, O'Sullivan KM, Jones LK, Lo C, Semple T, Kumanogoh A, et al. Endogenous CD100 promotes glomerular injury and macrophage recruitment in experimental crescentic glomerulonephritis. *Immunology.* 2009;128(1):114-22.
35. Ishida I, Kumanogoh A, Suzuki K, Akahani S, Noda K, and Kikutani H. Involvement of CD100, a lymphocyte semaphorin, in the activation of the human immune system via

CD72: implications for the regulation of immune and inflammatory responses. *Int Immunol.* 2003;15(8):1027-34.
36. Stewart BJ, Ferdinand JR, Young MD, Mitchell TJ, Loudon KW, Riding AM, et al. Spatiotemporal immune zonation of the human kidney. *Science.* 2019;365(6460):1461-6.
37. Arazi A, Rao DA, Berthier CC, Davidson A, Liu Y, Hoover PJ, et al. The immune cell landscape in kidneys of patients with lupus nephritis. *Nat Immunol.* 2019;20(7):902-14.
38. Bentham J, Morris DL, Graham DSC, Pinder CL, Tombleson P, Behrens TW, et al. Genetic association analyses implicate aberrant regulation of innate and adaptive immunity genes in the pathogenesis of systemic lupus erythematosus. *Nat Genet.* 2015;47(12):1457-64.
39. Zhang YM, Zhou XJ, Cheng FJ, Qi YY, Hou P, Zhao MH, et al. Association of the IKZF1 5' UTR variant rs1456896 with lupus nephritis in a northern Han Chinese population. *Scand J Rheumatol.* 2017;46(3):210-4.
40. Mackay F, Schneider P, Rennert P, and Browning J. BAFF AND APRIL: a tutorial on B cell survival. *Annu Rev Immunol.* 2003;21:231-64.
41. Avery DT, Kalled SL, Ellyard JI, Ambrose C, Bixler SA, Thien M, et al. BAFF selectively enhances the survival of plasmablasts generated from human memory B cells. *J Clin Invest.* 2003;112(2):286-97.
42. Ramanujam M, Bethunaickan R, Huang W, Tao H, Madaio MP, and Davidson A. Selective blockade of BAFF for the prevention and treatment of systemic lupus erythematosus nephritis in NZM2410 mice. *Arthritis Rheum.* 2010;62(5):1457-68.
43. Navarra SV, Guzman RM, Gallacher AE, Hall S, Levy RA, Jimenez RE, et al. Efficacy and safety of belimumab in patients with active systemic lupus erythematosus: a randomised, placebo-controlled, phase 3 trial. *Lancet.* 2011;377(9767):721-31.
44. Dooley MA, Houssiau F, Aranow C, D'Cruz DP, Askanase A, Roth DA, et al. Effect of belimumab treatment on renal outcomes: results from the phase 3 belimumab clinical trials in patients with SLE. *Lupus.* 2013;22(1):63-72.
45. Wu HJ, and Bondada S. Positive and negative roles of CD72 in B cell function. *Immunol Res.* 2002;25(2):155-66.
46. Radtke AJ, Chu CJ, Yaniv Z, Yao L, Marr J, Beuschel RT, et al. IBEX: an iterative immunolabeling and chemical bleaching method for high-content imaging of diverse tissues. *Nat Protoc.* 2022;17(2):378-401.
47. Radtke AJ, Kandov E, Lowekamp B, Speranza E, Chu CJ, Gola A, et al. IBEX: A versatile multiplex optical imaging approach for deep phenotyping and spatial analysis of cells in complex tissues. *Proc Natl Acad Sci U S A.* 2020;117(52):33455-65.
48. Wolf FA, Angerer P, and Theis FJ. SCANPY: large-scale single-cell gene expression data analysis. *Genome Biol.* 2018;19(1):15.
49. Stuart T, Butler A, Hoffman P, Hafemeister C, Papalexi E, Mauck WM, 3rd, et al. Comprehensive Integration of Single-Cell Data. *Cell.* 2019;177(7):1888-902 e21.
50. Wolock SL, Lopez R, and Klein AM. Scrublet: Computational Identification of Cell Doublets in Single-Cell Transcriptomic Data. *Cell Syst.* 2019;8(4):281-91 e9.
51. Popescu DM, Botting RA, Stephenson E, Green K, Webb S, Jardine L, et al. Decoding human fetal liver haematopoiesis. *Nature.* 2019;574(7778):365-71.

52. Benjamini Y, and Hochberg Y. Controlling the False Discovery Rate: A Practical and Powerful Approach to Multiple Testing. *Journal of the Royal Statistical Society: Series B (Methodological).* 1995;57(1):289-300.
53. Polanski K, Young MD, Miao Z, Meyer KB, Teichmann SA, and Park JE. BBKNN: fast batch alignment of single cell transcriptomes. *Bioinformatics.* 2020;36(3):964-5.
54. Traag VA, Waltman L, and van Eck NJ. From Louvain to Leiden: guaranteeing well-connected communities. *Sci Rep.* 2019;9(1):5233.
55. McInnes L, Healy J, and Melville J. Umap: Uniform manifold approximation and projection for dimension reduction. *arXiv preprint arXiv:180203426.* 2018.
56. Aibar S, Gonzalez-Blas CB, Moerman T, Huynh-Thu VA, Imrichova H, Hulselmans G, et al. SCENIC: single-cell regulatory network inference and clustering. *Nat Methods.* 2017;14(11):1083-6.
57. Subramanian A, Tamayo P, Mootha VK, Mukherjee S, Ebert BL, Gillette MA, et al. Gene set enrichment analysis: A knowledge-based approach for interpreting genome-wide expression profiles. *Proceedings of the National Academy of Sciences.* 2005;102(43):15545-50.
58. Liberzon A, Subramanian A, Pinchback R, Thorvaldsdóttir H, Tamayo P, and Mesirov JP. Molecular signatures database (MSigDB) 3.0. *Bioinformatics.* 2011;27(12):1739-40.
59. Dhodapkar KM, Banerjee D, Connolly J, Kukreja A, Matayeva E, Veri MC, et al. Selective blockade of the inhibitory Fcgamma receptor (FcgammaRIIB) in human dendritic cells and monocytes induces a type I interferon response program. *J Exp Med.* 2007;204(6):1359-69.
60. Baechler EC, Batliwalla FM, Karypis G, Gaffney PM, Ortmann WA, Espe KJ, et al. Interferon-inducible gene expression signature in peripheral blood cells of patients with severe lupus. *Proc Natl Acad Sci U S A.* 2003;100(5):2610-5.
61. Xue J, Schmidt SV, Sander J, Draffehn A, Krebs W, Quester I, et al. Transcriptome-based network analysis reveals a spectrum model of human macrophage activation. *Immunity.* 2014;40(2):274-88.
62. Castro-Dopico T, Dennison TW, Ferdinand JR, Mathews RJ, Fleming A, Clift D, et al. Anti-commensal IgG Drives Intestinal Inflammation and Type 17 Immunity in Ulcerative Colitis. *Immunity.* 2019;50(4):1099-114.e10.
63. Friedman JH, Hastie T, and Tibshirani R. Regularization Paths for Generalized Linear Models via Coordinate Descent. *2010.* 2010;33(1):22.
64. Street K, Risso D, Fletcher RB, Das D, Ngai J, Yosef N, et al. Slingshot: cell lineage and pseudotime inference for single-cell transcriptomics. *BMC genomics.* 2018;19(1):477.
65. Van den Berge K, Roux de Bézieux H, Street K, Saelens W, Cannoodt R, Saeys Y, et al. Trajectory-based differential expression analysis for single-cell sequencing data. *Nat Commun.* 2020;11(1):1201.
66. Van de Sande B, Flerin C, Davie K, De Waegeneer M, Hulselmans G, Aibar S, et al. A scalable SCENIC workflow for single-cell gene regulatory network analysis. *Nat Protoc.* 2020;15(7):2247-76.
67. Efremova M, Vento-Tormo M, Teichmann SA, and Vento-Tormo R. CellPhoneDB: inferring cell–cell communication from combined expression of multi-subunit ligand–receptor complexes. *Nature Protocols.* 2020;15(4):1484-506.

Figures and figure legends

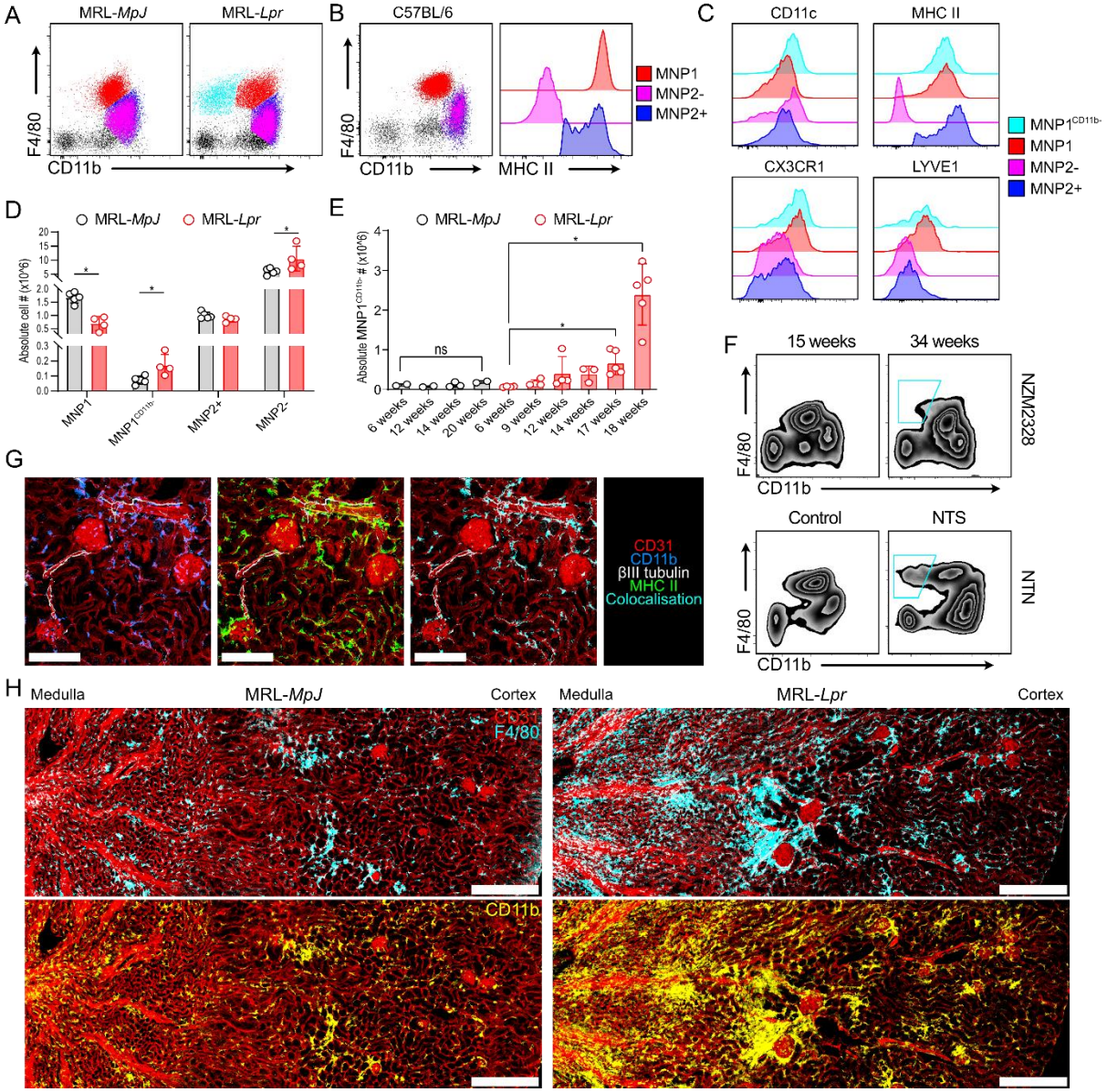

Figure 1. Expanded kidney macrophage populations in lupus nephritis. (**A**) Representative CD11b vs F4/80 expression by kidney MNPs in MRL-*MpJ* (left) and MRL-*Lpr* (right) mice. (**B**) Representative CD11b vs F4/80 and MHC II expression by kidney MNPs in C57BL/6 mice with cells identified as MNP1 (F4/80^{hi}, CD11b^{int} MHC II^{hi}), MNP2+ (F4/80^{int} CD11b^{hi} MHC II+) and MNP2- (F4/80^{int} CD11b^{hi} MHC II-). (**C**) Surface expression of CD11c, MHC II, CX3CR1 and LYVE1 by kidney MNP subsets in MRL mice. (**D**) Absolute cell numbers of kidney MNPs in 16-week-old MRL-*MpJ* and MRL-*Lpr* mice. n = 5-6 animal per group from two separate experiments . *p<0.05, Student t-test. (**E**) Absolute numbers of MNP1^{CD11b-} per kidney in MRL-*MpJ* and MRL-*Lpr* mice with age. n = 2-5 animals per group. *p<0.05, Student t-test. (**F**) Representative CD11b and F4/80 expression by kidney MNPs in young and old NZM2328 mice (top, n = 5) and following administration of nephrotoxic serum in C57BL/6 mice (bottom, n = 6). (**G**) Representative confocal microscopy (n = 3) on murine

C57BL/6 kidney showing MNP distribution around peritubular, afferent/efferent blood vessels and glomeruli (CD31, red) as well as surrounding nerves (βIII tubulin, white) through expression of CD11b (blue) and MHC II (green). Scale bar = 150μm. (**H**) Representative confocal microscopy (n = 4) showing MNP distribution in kidneys from 18-week-old MRL-*MpJ* (left) and MRL-*Lpr* (right) mice through expression of F4/80 (cyan) and CD11b (yellow) relative to blood vessels (CD31, red). Scale bar = 300μm.

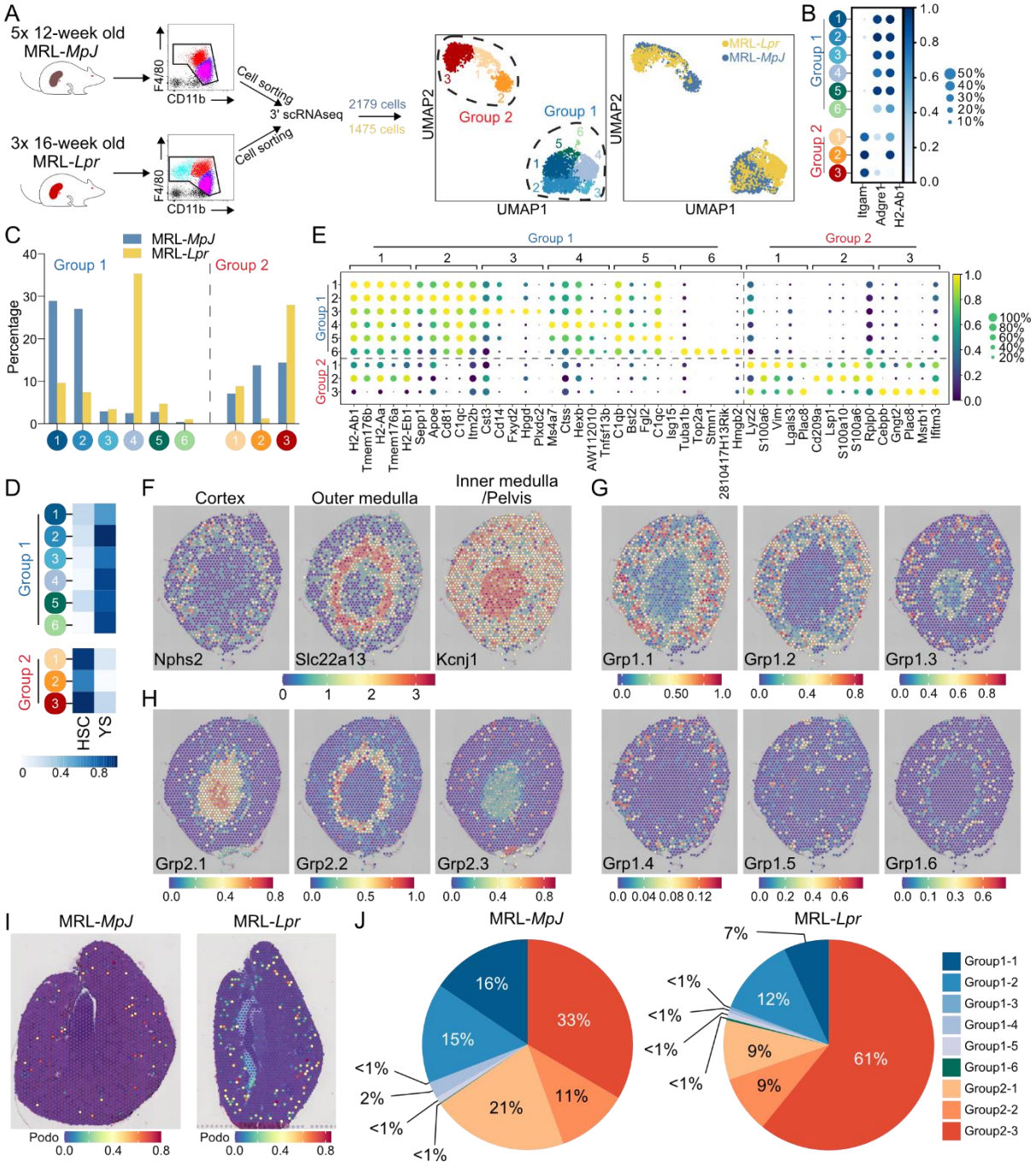

Figure 2. Nephritis-associated macrophage heterogeneity at single cell resolution. (**A**) Illustration of single-cell experiment set up (left panels) and UMAP embedding of 2179 macrophages from MRL-*MpJ* and 1475 macrophages from MRL-*Lpr* mice (right panels). (**B**) Mean expression dot plot of genes Itgam (CD11b), Adgre1 (F4/80) and H2-Ab1 (MHC II). (**C**) Proportion of cells found in each cluster and mouse strain. (**D**) Heatmap of mean AUCell enrichment of F4/80hi/lo gene sets, corresponding to yolk sac (YS) vs hematopoietic stem-cell (HSC) lineage. (**E**) Mean expression dot plot of top five significant marker genes for each MNP cluster. Marker genes were identified using Wilcoxon rank sum test and p adj < 0.05 was considered statistically significant. (**F**) Spatial expression of markers used to

delineate the anatomical regions in Visium Spatial Gene Expression data of C57BL/6 kidney sections (Kcnj1 – pelvis; Slc22a13 – proximal tubules and Nphs2 – glomeruli). (**G**) Spatial transcriptomics of Group 1 macrophages signatures in C57BL/6 murine kidneys with annotated scRNAseq data above. Each spot / voxel denotes a prediction score of 0 – 1 for the location of each of the macrophage subgroups. (**H**) Spatial transcriptomics of Group 2 macrophages signatures in C57BL/6 murine kidneys with annotated scRNAseq data above. Each spot / voxel denotes a prediction score of 0 – 1 for the location of each of the macrophage subgroups. (**I**) Spatial transcriptomics of podocyte signature in MRL-*MpJ* (left) and MRL-*Lpr* (right) kidneys to identify glomerulus-containing spots/voxels. (**J**) Average proportion of each macrophage subset signature in spots/voxels identified in (I) in the MRL-*MpJ* (left) and MRL-*Lpr* (right) kidneys.

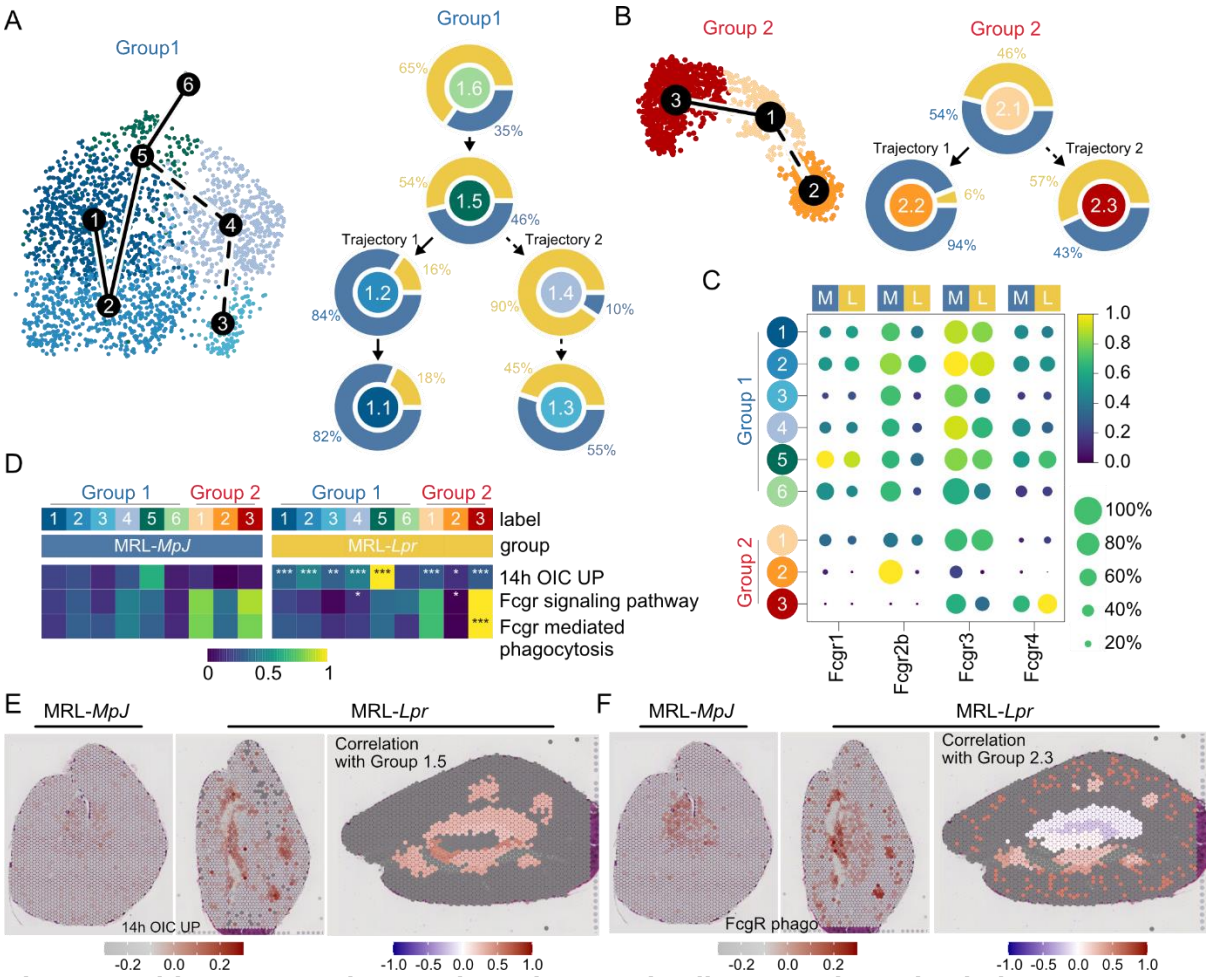

Figure 3. Kidney macrophages show deranged cell state trajectories in lupus nephritis. (**A**) (Left) UMAP embedding of Group 1 cells with summary tracks of slingshot trajectory connecting the Group 1 clusters. (Right) Proportion of cells from MRL-*MpJ* (blue) or MRL-*Lpr* (yellow) from each cluster organized according to predicted trajectory. (**B**) (Left) UMAP embedding of Group 2 cells with summary tracks of slingshot trajectory connecting the Group 2 clusters. (Right) Proportion of cells from MRL-*MpJ* (blue) or MRL-*Lpr* (yellow) from each cluster organized according to predicted trajectory. (**C**) Mean expression dot plot of Fc gamma receptor genes split by mouse strain (M = MRL-*MpJ*; L = MRL-*Lpr*). (**D**) Heatmap of mean AUCell enrichment of immune complex stimulation/cross-linking related gene sets split by MRL-*MpJ* or MRL-*Lpr*. Statistical significance testing was performed using pairwise Wilcoxon rank sum tests and adjusted with bonferonni post-test where *p<0.05; **p<0.01; ***p<0.001. (**E**) (Left and middle panels) Spatial expression of immune complex stimulation/cross-linking related gene sets in Visium Spatial Gene Expression data of MRL-*MpJ* (left) and MRL-*Lpr* (right) kidney sections. (Right panel) Positive correlation values of expression of gene set with Group 1.5 prediction scores across k-nearest neighborhoods of spots are colored from white to red. Grey spots indicate no available scores or negative correlation. (**F**) (Left and middle panels) Spatial expression of FcγR-mediated phagocytosis related gene sets in Visium Spatial Gene Expression data of MRL-*MpJ* (left) and MRL-*Lpr*

(right) kidney sections. (Right panel) Positive correlation values of expression of gene set with Group 2.3 prediction scores across k-nearest neighborhoods of spots are colored from white to red. Grey spots indicate no available scores or negative correlation.

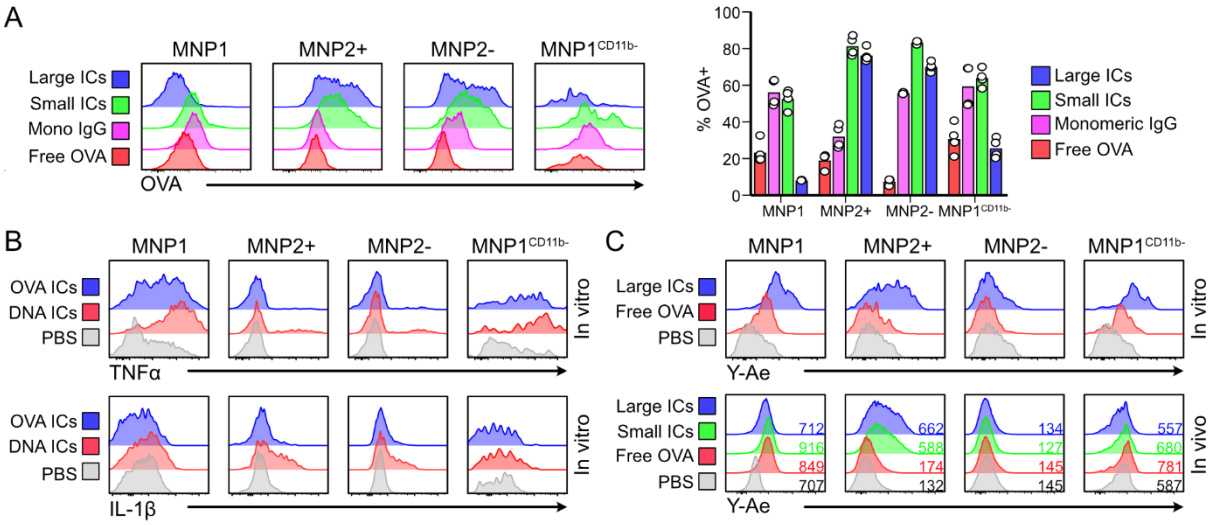

Figure 4: Kidney macrophages produce cytokines and present antigen upon IC uptake. (**A**) (Left) Uptake of free and immune complexed AF647-OVA by kidney MNPs in vivo 2h following intravenous injection in C57BL/6 mice. 5:1 (large), 1:1 (small) and 1:5 (monomeric) molar ratios of rabbit IgGs:OVA were used. (Right) Uptake of free and immune complexed AF647-OVA by kidney MNPs in vivo 2h following intravenous injection in C57BL/6 mice. n = 2-4 mice per group from two separate experiments (**B**) Representative expression (n = 3) of TNFα (top) and IL-1β (bottom) by each MNP subset after 2h of stimulation in vitro with the appropriate condition. (**C**) Antigen presentation by kidney MNPs in vitro (top, n = 3) 2h following stimulation with free or immune complexed Eα-AF647-OVA or in vivo (bottom, n = 4-6 from two separate experiments) 4h following intravenous injection of free or immune complexed Eα-AF647-OVA in C57BL/6 mice. The number indicates the average gMFI for this channel.

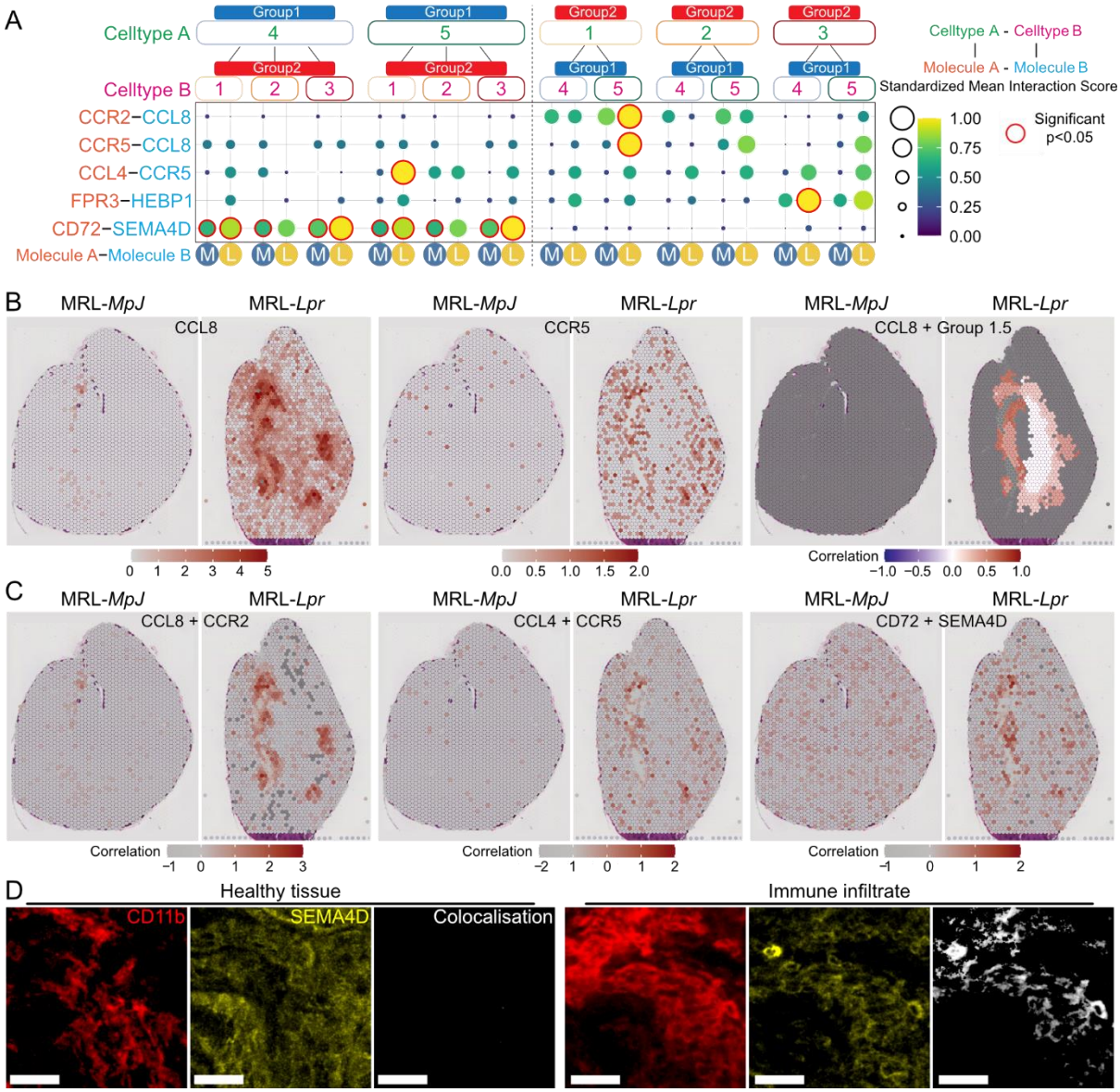

Figure 5. Tissue-resident macrophages orchestrate monocyte-recruitment in lupus nephritis. (**A**) CellPhoneDB receptor-ligand interaction analysis between Group 1 (Group 1.4 and Group 1.5) and Group 2 (Group 2.1, Group 2.2 and Group 2.3) clusters split by mouse strain (M = MRL-*MpJ*; L = MRL-*Lpr*). Significant interactions ($p < 0.05$) are highlighted in red. (**B**) Spatial expression of CCL8 and CCR5 in Visium Spatial Gene Expression data of MRL-*MpJ* (left) and MRL-*Lpr* (right) kidney sections. (Left and middle) Expression of molecules per spot are colored from increasing gradient from white to red and corresponds to increasing expression value. (Right) Positive correlation values of expression of molecules with Group 1.5 prediction scores across k-nearest neighborhoods of spots are colored from white to red. Grey spots indicate no available scores or negative correlation. (**C**) Positive correlation values of expression of molecules (CCL8 and CCR2, left; CCL4 and CCR5, middle; CD72 and SEMA4D, right) in Visium Spatial Gene Expression data of MRL-*MpJ* (left) and MRL-*Lpr* (right) kidney sections. Positive correlation values of expression of

molecules are colored from white to red. Grey spots indicate no available scores or negative correlation. (**D**) Representative confocal microscopy (n = 3) showing SEMA4D expression (yellow) in a large immune infiltrate (left) and a healthy region of the cortex (right) (CD11b – red, F4/80 – cyan) in the kidneys from 18-week-old MRL-*Lpr* mice. Colocalisation of CD11b with SEMA4D shown in white. Scale bar = 25µm.

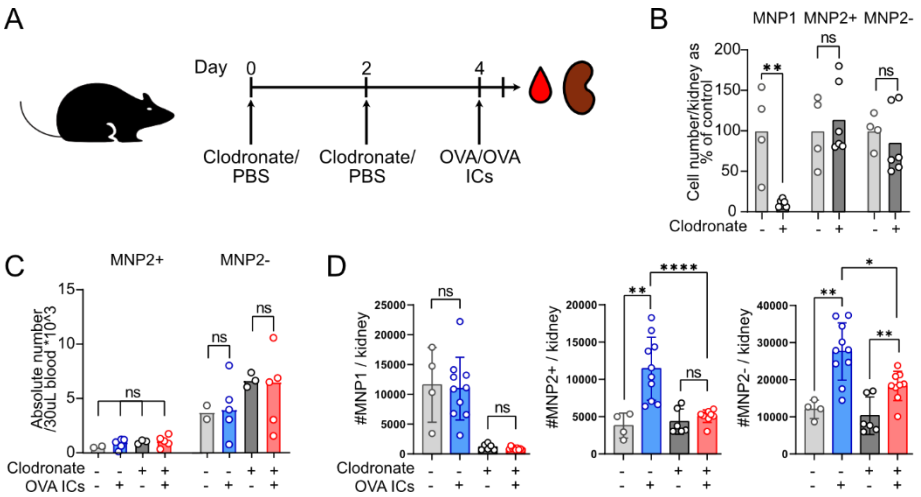

Figure 6: Tissue-resident macrophages orchestrate IC-dependent monocyte recruitment. (**A**) Illustration of the experimental set up for in vivo experiment. (**B**) Numbers of MNP1 and MNP2 subsets in the kidneys following two injections of liposome clodronate shown as percentage of cells in the control (PBS injected) kidneys. n = 4-6 per group. **p<0.01, Mann-Whitney test with Benjamini, Krieger and Yekutieli post-test applied. (**C**) Absolute number of CD11b^{hi} MHC II+ (MNP2+) and MHC II- (MNP2-) cells in 30µL of blood 4h following injection of free or complexed ovalbumin in mice that had received clodronate or PBS as described in figure 3E. n = 2-5 per group (**D**) Absolute numbers for each MNP subset 4 hours following i.v. injection of free or immune complexed ovalbumin (right) for each experimental condition in the kidneys. n = 4-10 per group. *p<0.05, **p<0.01, ***p<0.001, ****p<0.0001, Mann-Whitney test with Benjamini, Krieger and Yekutieli post-test applied.

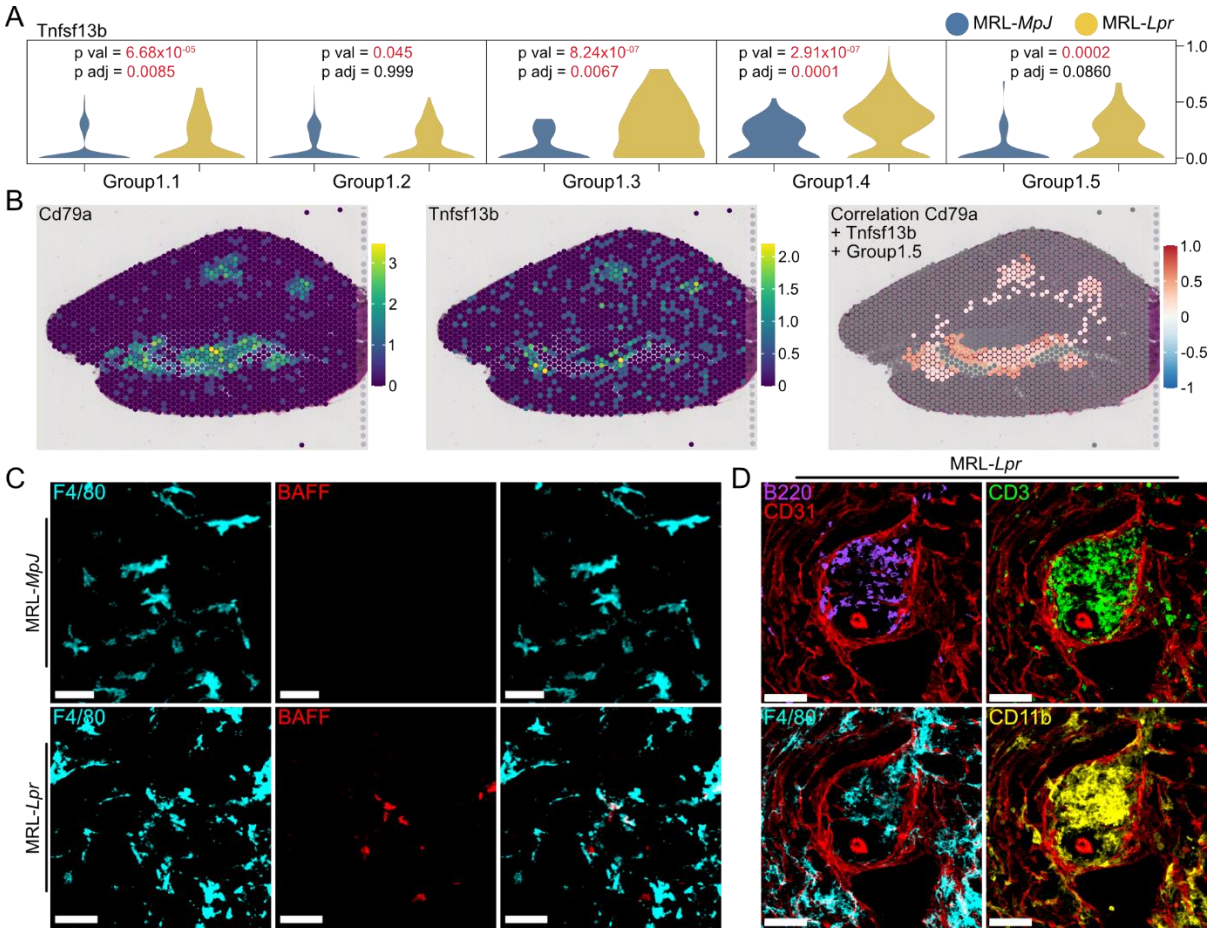

Figure 7. Tissue-resident macrophages produce B cell cytokine. (**A**) Violin plot of Tnfsf13b (BAFF) in Group 1 clusters. (**B**) Spatial expression of Cd79a and Tnfsf13b in Visium Spatial Gene Expression data of MRL-*Lpr* kidney section. (Left and middle) Expression of molecules per spot are colored from increasing gradient from purple to green to yellow and corresponds to increasing expression value. (Right) Positive correlation values of expression of molecules with Group 1.5 prediction scores across k-nearest neighborhoods of spots are colored from white to red. Grey spots indicate no available scores or negative correlation. (**C**) Representative confocal microscopy (n = 3 per group) showing BAFF expression (red) in macrophages (F4/80, cyan) in kidneys from 18-week-old MRL-*MpJ* (top) and MRL-*Lpr* (bottom) mice. Scale bar = 30µm. (**D**) Representative confocal microscopy (n = 3) showing immune infiltrates containing B (B220, purple) and T (CD3, green) cells alongside F4/80+ (cyan) and CD11b+ (yellow) MNPs around blood vessels (CD31, red) in kidneys from MRL-*Lpr* mice. Scale bar = 70µm.

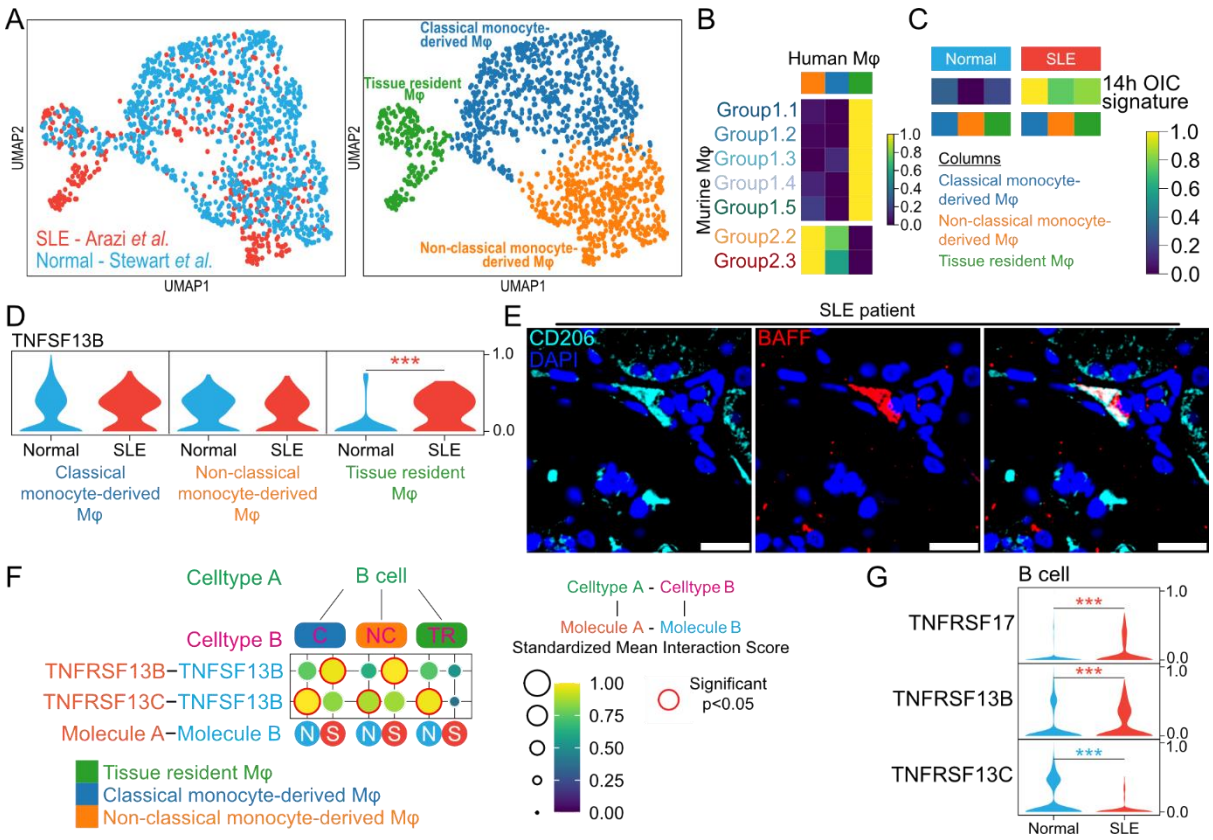

Figure 8: Human kidney MNP show perturbations in FcγR expression, activation and interactions in lupus nephritis. (**A**) Integrated UMAP embedding of macrophages from publicly available datasets of human kidneys (normal and SLE). (**B**) Heatmap of mean AUCell enrichment of mouse Group1 and Group2 signatures in human macrophage clusters. (**C**) Heatmap of mean AUCell enrichment of opsonised immune complex (OIC) cross linking signature split by normal or SLE. (**D**) Violin plot of Tnfsf13b in human macrophage clusters. Expression value is scaled from 0 to 1 across cell clusters. Significance was calculated using Wilcoxon rank sum test with BH post-test applied where ***p<0.001. Colour of the p-value indicates which group has a higher value (red = SLE, blue = normal). (**E**) Microscopy showing BAFF expression (red) in peri-glomerular macrophage (CD206, cyan) in kidneys from SLE patients. Scale bar = 20µm. (**F**) CellPhoneDB receptor-ligand interaction analysis between human B cells and human macrophage clusters (NC – non-classical monocyte-derived macrophages; C – classical monocyte-derived macrophages; TR – tissue resident macrophages) split by normal (N) or SLE (S). Significant interactions ($p < 0.05$) are highlighted in red. (**G**) Violin plot of BAFF receptor molecules in human B cells. Expression value is scaled from 0 to 1. Significance was calculated using Wilcoxon rank sum test with BH post-test applied where *p<0.05; ***p<0.001. Colour of the p-value indicates which group has a higher value (red = SLE, blue = normal).

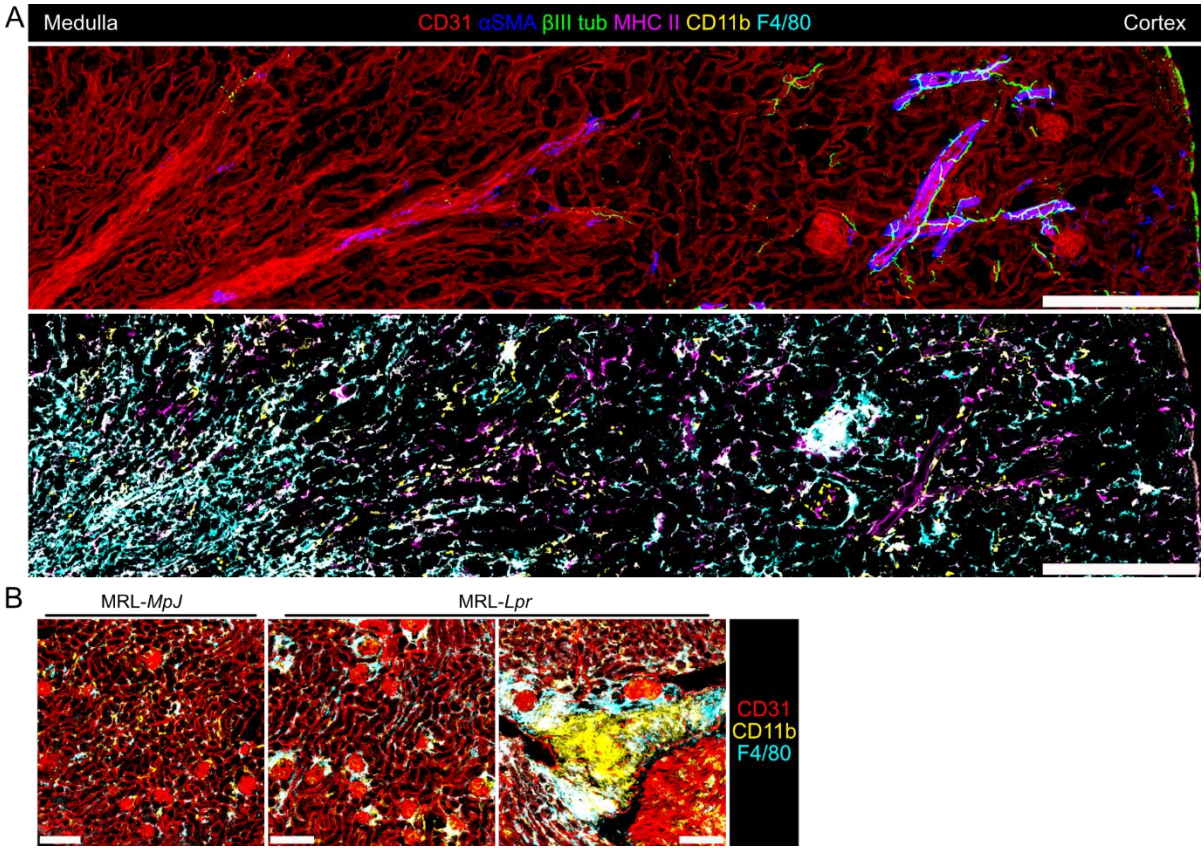

Supplemental figure 1: Macrophage populations expand with inflammation. (**A**) Representative iterative staining (n = 3) on murine C57BL/6 kidney showing MNP distribution throughout the tissue through expression of F4/80 (cyan), CD11b (yellow) and MHC II (magenta) (bottom) relative to blood vessels (CD31, red) and surrounding smooth muscles (αSMA, blue) and nerves (βIII tubulin, green) (top). Scale bar = 350μm (**B**) Representative confocal microscopy (n = 3 per group) showing MNP distribution in kidneys from 18-week-old MRL-*MpJ* (left) and MRL-*Lpr* (middle and right) mice through expression of F4/80 (cyan) and CD11b (yellow) relative to blood vessels (CD31, red). Scale bar = 150μm.

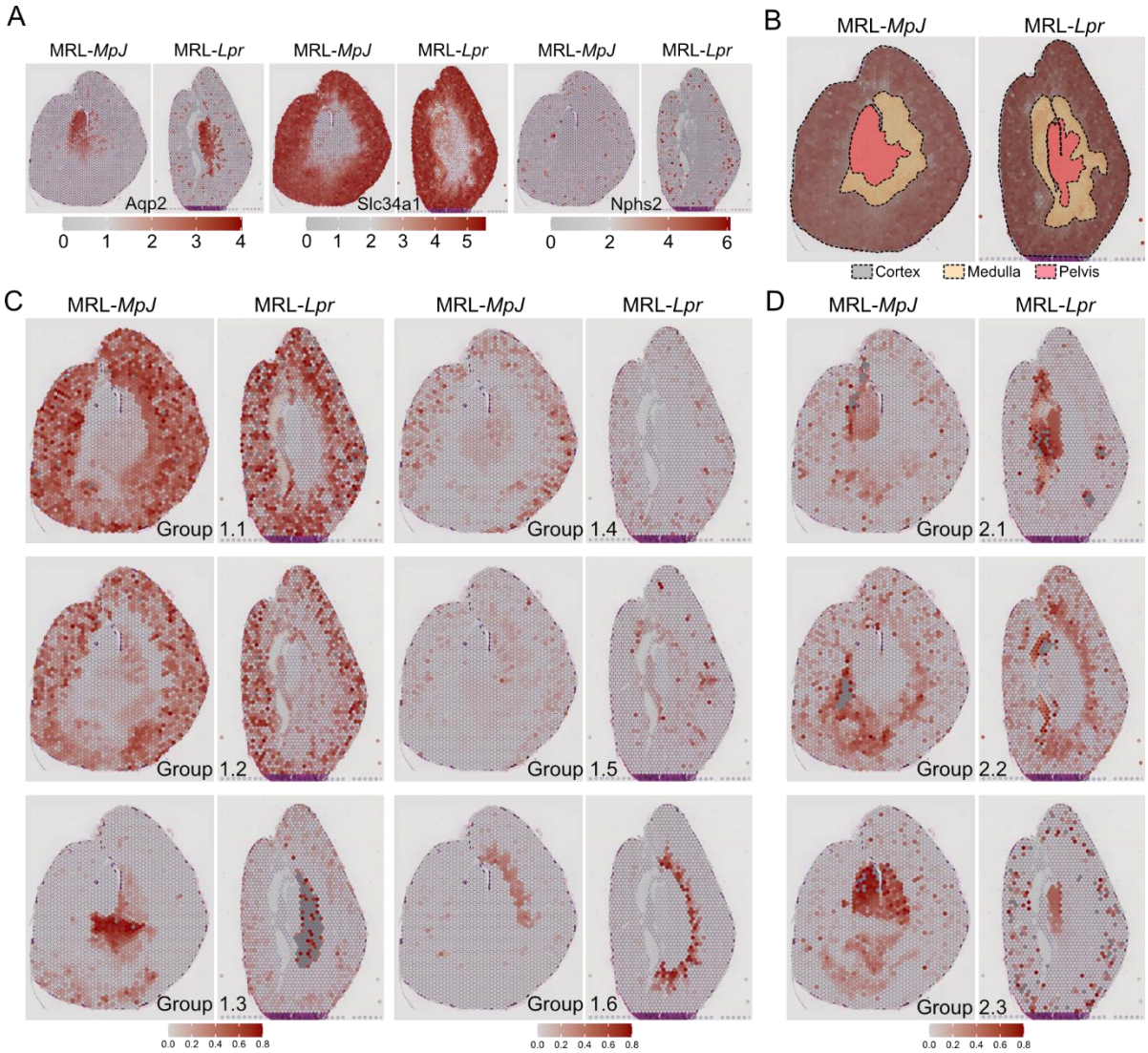

Supplemental figure 2: Spatial distribution of kidney macrophage populations. (**A**) Spatial expression of markers used to delineate the anatomical regions in Visium Spatial Gene Expression data of MRL-*MpJ* and MRL-*Lpr* kidney sections (Aqp2 – pelvis; Slc34a1 = proximal tubules and Nphs2 – glomeruli). (**B**) Delineation of anatomical regions in MRL-*MpJ* and MRL-*Lpr* visium kidney sections based on (A). (**C**) Spatial transcriptomics of Group 1 macrophages signatures in MRL-*MpJ* and MRL-*Lpr* murine kidneys with annotated scRNAseq data above. Each spot / voxel denotes a prediction score of 0 – 1 for the location of each of the macrophage subgroups. (**D**) Spatial transcriptomics of Group 2 macrophages signatures in MRL-*MpJ* and MRL-*Lpr* murine kidneys with annotated scRNAseq data above. Each spot / voxel denotes a prediction score of 0 – 1 for the location of each of the macrophage subgroups.

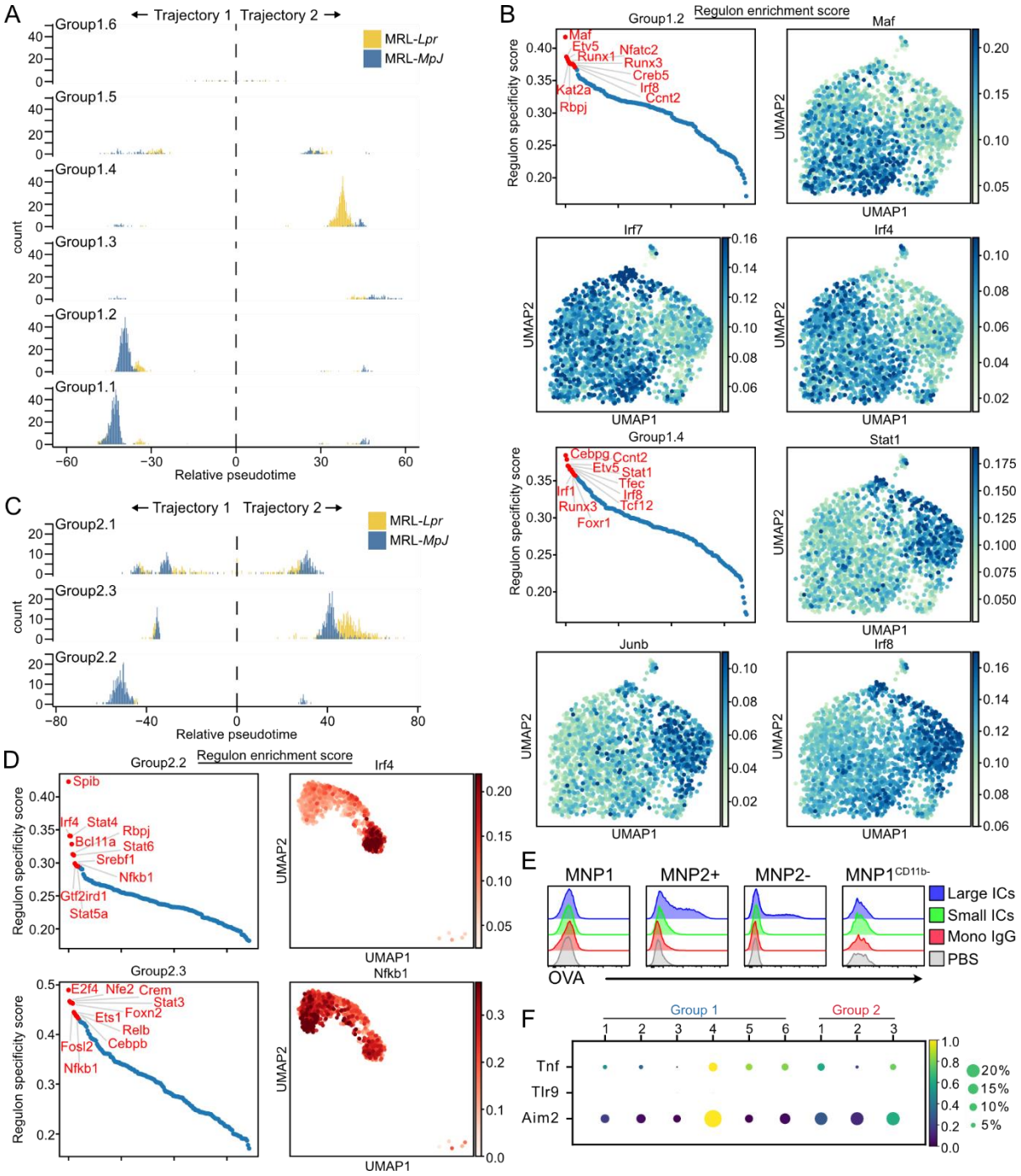

Supplemental figure 3: Trajectory and regulon analysis of kidney macrophages. (**A**) Proportion of cells from MRL-*MpJ* (blue) or MRL-*Lpr* (yellow) from each Group 1 cluster distributed along pseudotime scale. (**B**) (Top) Top ranked regulons in trajectory 1 for Group 1 (left) and enrichment UMAP of regulon activity of Maf, Irf7 and Irf4 in Group 1.2 trajectory (trajectory 1). (Bottom) Top ranked regulons in trajectory 2 for Group 1 (left) and enrichment UMAP of regulon activity of Stat1, Junb and Irf8 in Group 1.4 trajectory (trajectory 2). (**C**) Proportion of cells from MRL-*MpJ* (blue) or MRL-*Lpr* (yellow) from each Group 2 cluster distributed along pseudotime scale. (**D**) (Top left) Top ranked regulons in trajectory 1 for Group 2. (top right) Enrichment UMAP of regulon activity of Irf4 in Group 2.2 trajectory

(trajectory 1). (Bottom left) Top ranked regulons in trajectory 2 for Group 2. (Bottom right) Enrichment UMAP of regulon activity of Nfkb1 in Group 2.3 trajectory (trajectory 2). (**E**) Uptake of free and immune complexed AF647-OVA by kidney MNPs in vivo 2h following intravenous injection in C57BL/6 mice. 5:1 (large) and 1:1 (small) molar ratios of mouse IgGs:OVA were used. (**F**) Mean expression dot plot of genes Tnf, Tlr9 and Aim2.

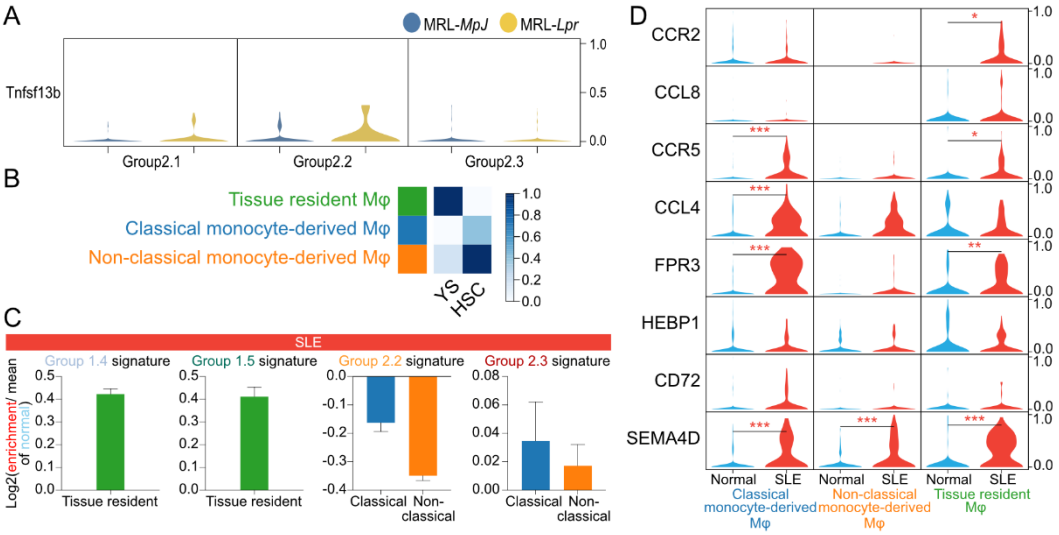

Supplemental figure 4: Kidney macrophages in human SLE. (**A**) Violin plot of Tnfsf13b (BAFF) in Group 2 clusters. (**B**) Heatmap of mean AUCell enrichment of F4/80hi/lo gene sets, corresponding to yolk sac (YS) vs hematopoetic stem-cell (HSC) lineage. Row enrichment value is scaled from 0 to 1 and presented as an increasing gradient from white to blue which corresponds to increasing enrichment score. (**C**) Bar charts showing relative log2 difference of AUCell enrichment of mouse Group1 and Group2 macrophage clusters in SLE compared to normal (mean of normal enrichment used as reference). (**D**) Violin plot of molecules, with significant interactions found in mouse macrophage in (A), in human macrophage clusters. Expression value is scaled from 0 to 1 across cell clusters. Significance was calculated using Wilcoxon rank sum test with BH post-test applied where *p<0.05; ***p<0.001. Colour of the p-value indicates which group has a higher value (red = SLE, blue = normal).

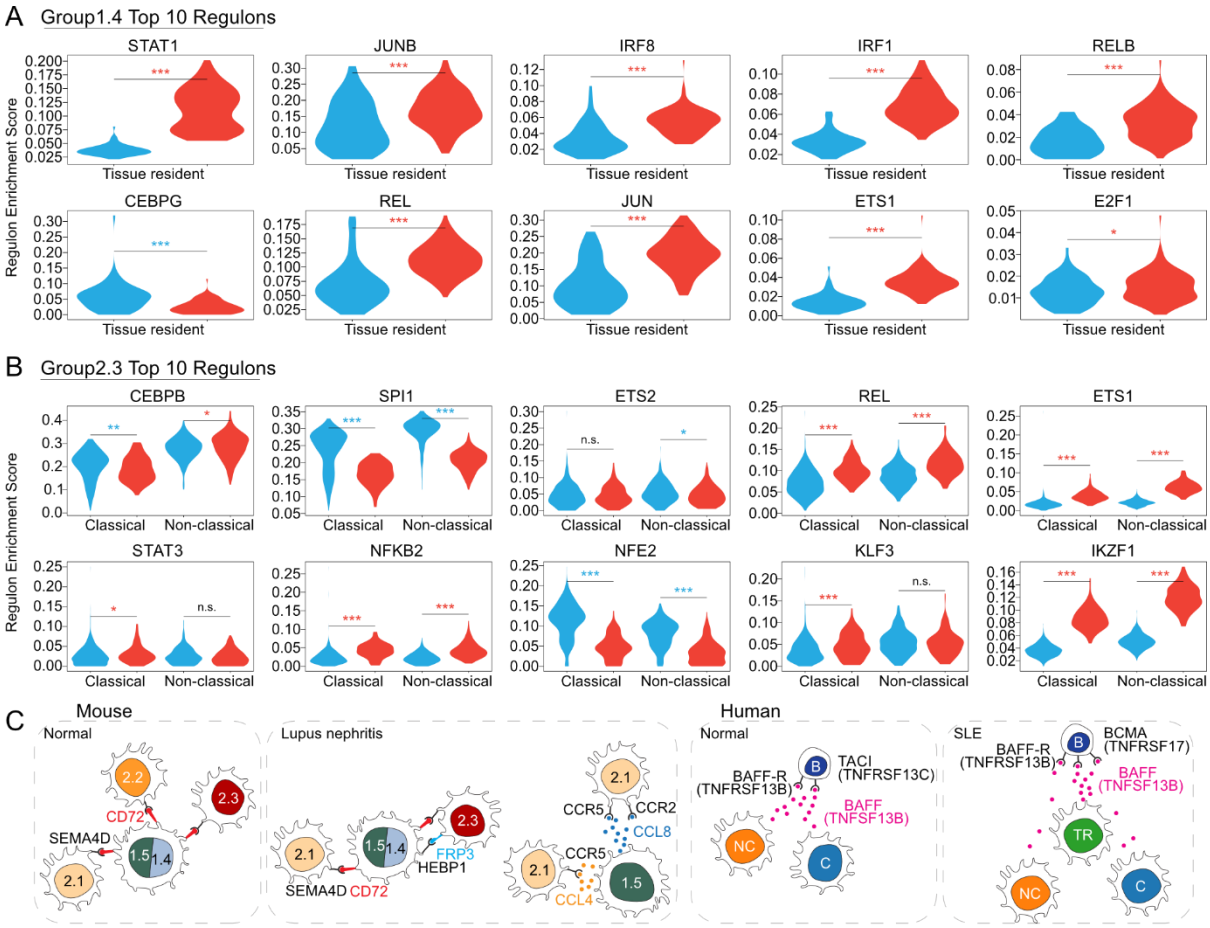

Supplemental figure 5: Top regulons in kidney macrophages. (**A**) Violin plot of regulon enrichment scores in human tissue resident macrophages split by normal (blue) or SLE (red) for Group1.4-related top 10 transcription factors. Significance was calculated using Wilcoxon rank sum test with BH post-test applied where *p<0.05; ***p<0.001. Colour of the p-value indicates which group has a higher value (red = SLE, blue = normal). (**B**) Violin plot of regulon enrichment scores in human monocyte-derived macrophages split by normal (blue) or SLE (red) for Group2.3-related top 10 transcription factors. Significance was calculated using Wilcoxon rank sum test with BH post-test applied where *p<0.05; ***p<0.001. Colour of the p-value indicates which group has a higher value (red = SLE, blue = normal). (**C**) Summary illustration of macrophage interactions in mouse and human kidneys.

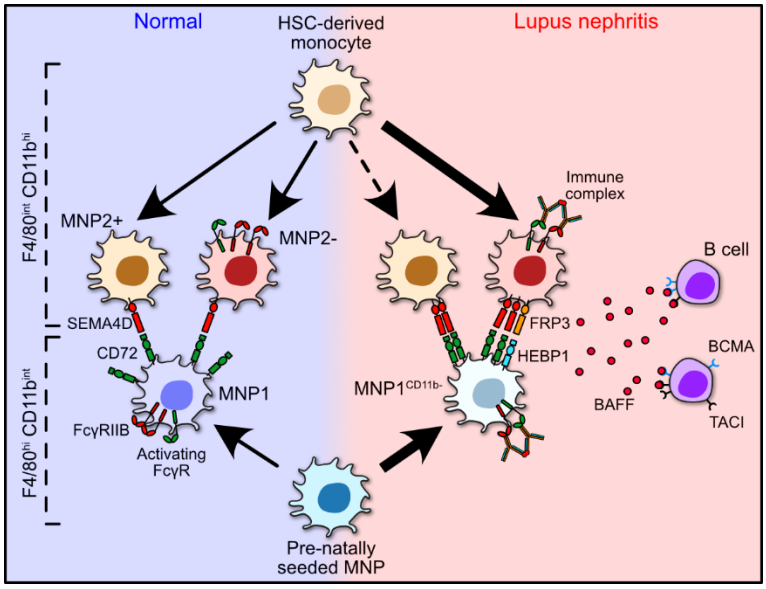

Graphical abstract

						Dilution	
Marker	Conjugate	Clone	Cat#	Vendor	Target	Flow cytometry	Microscopy
α-SMA	AF488	1A4	ab184675	Abcam	Mouse	x	1/100
B220	AF647	RA3-6B2	557683	BD Biosciences	Mouse	x	1/200
BAFF	x	Polyclonal	AF124	R&D systems	Human		
BAFF	x	Polyclonal	bs-2431R	Thermo	Mouse	x	1/50
βIII tubulin	AF488	TUJ1	801203	BioLegend	Mouse	x	1/100
CD3	AF488	17A2	100210	BioLegend	Mouse	x	1/100
CD3ε	Pacific Blue	145-2C11	48-0031-82	Invitrogen	Mouse	1/50	x
CD3ε	APC	145-2C11	17-0031-82	Invitrogen	Mouse	1/50	x
CD11b	PE	M1/70	101208	BioLegend	Mouse	x	1/50
CD11b	PerCP-Cy5.5	M1/70	45-0112-82	Invitrogen	Mouse	1/500	x
CD11c	PE	N418	117308	BioLegend	Mouse	1/100	x
CD16	APC	S17014E	158005	BioLegend	Mouse	1/50	x
CD16.2	PE	9E9	149503	BioLegend	Mouse	1/200	x
CD19	eF450	eBio1D3	48-0193-82	Invitrogen	Mouse	1/100	x
CD31	PE	MEC13.3	102520	BioLegend	Mouse	x	1/100
CD31	AF594	MEC13.3	553373	BD Biosciences	Mouse	x	1/100
CD32b	PE	AT130-2	12-0321-82	Invitrogen	Mouse	1/200	x
CD45	APC-eF780	30-F11	47-0451-82	Invitrogen	Mouse	1/200	x
CD45 i.v.	FITC	30-F11	11-0451-82	Invitrogen	Mouse	x	x
CD64	PE	X54-5/7.1	139304	BioLegend	Mouse	1/100	x
CD86	PE	GL-1	105007	BioLegend	Mouse	1/100	x
CD206	PE-Dazzle	C068C2	141732	BioLegend	Human	x	1/100
CX3CR1	PE	SA011F11	149006	BioLegend	Mouse	1/100	x
F4/80	AF647	F4/80	ab204467	Abcam	Mouse	x	1/50
F4/80	PE-Cy7	BM8	25-4801-82	Invitrogen	Mouse	1/200	x
Gr1	Pacific Blue	RB6-8C5	48-5931-82	Invitrogen	Mouse	1/2000	x
LYVE1	Biotin	ALY7	13-0443-82	Invitrogen	Mouse	1/100	x
MHC II	eF450	M5/114.15.2	48-5321-82	Invitrogen	Mouse	x	1/50
MHC II	BV650	M5/114.15.2	107641	BioLegend	Mouse	1/400	x
NK1.1	Pacific Blue	PK136	108722	BioLegend	Mouse	1/50	x
SEMA4D	AF594	BMA-12	147609	BioLegend	Mouse	x	1/50
Y-Ae	Biotin	eBioY-Ae	13-5741-82	Invitrogen	Mouse	1/50	x
Anti-rabbit IgG	AF488	Polyclonal	A32790	Invitrogen	x	x	1/200
Hoecht 33258	x	x	40044	Biotum	x	x	1/5 000
Live/Dead	Aqua	x	L34957	Thermo	x	1/250	x
Streptavidin	PE	x	12-4317-87	Invitrogen	x	1/200	x

Table S1: Antibodies used for microscopy and flow cytometry in this study.